Gravity Compensation of an Exoskeleton Joint Using Constant-Force Springs

A Thesis

Presented in Partial Fulfillment of the Requirements for the

Degree of Master of Science

with a

Major in Mechanical Engineering

in the

College of Graduate Studies

University of Idaho

Parker W. Hill

Major Professor: Eric Wolbrecht, Ph.D.

Committee Members: Joel Perry, Ph.D, Michael Maughan, Ph.D

Department Administrator: Steven Beyerlein, Ph.D

August 2019

Authorization to Submit Thesis

This thesis of Parker W. Hill, submitted for the degree of Master of Science with a Major in Mechanical Engineering and titled "Gravity Compensation of an Exoskeleton Joint Using Constant-Force Springs" has been reviewed in final form. Permission, as indicated by the signatures and dates below, is now granted to submit final copies to the College of Graduate Studies for approval.

Major Professor: _____ Date: _____
Eric T. Wolbrecht, Ph.D.

Committee Members: _____ Date: _____
Joel C. Perry, Ph.D

_____ Date: _____
Michael Maughan, Ph.D

Department Administrator: _____ Date: _____
Steven Beyerlein, Ph.D

Abstract

Stroke is one of the leading causes of impairment in the world. Many of those who have suffered a stroke experience long-term loss of upper-limb function as a result. BLUE SABINO is an exoskeleton device being developed at the University of Idaho to help assess these patients and aid in their rehabilitation. One of the central design challenges with exoskeletons is limiting the overall weight of the device. Motors used in actuation of these devices are often oversized to allow for gravity compensation and the creation of torques that facilitate patient movements. However, if the torques required for gravity compensation are achieved through passive elastic elements, the motor and other upstream components can be lighter, potentially greatly reducing the overall weight of the device. In this paper, constant-force springs are investigated as a method of generating a constant offsetting torque to compensate for gravity. In experimental testing of multiple mounting configurations of constant-force springs (single, back-to-back, double-wrapped), the force output fluctuated less than 8.6% over 180° of wrapping, with friction values below 2.6%, validating the viability of constant-force springs for this application. The results suggest that when using multiple springs, the back-to-back configuration provides a simpler implementation with better force consistency while the double-wrapped configuration adds less friction to the system. With these results, a mechanism was created to provide a torque of 35 ± 0.7 N-m to joint 3 of the BLUE SABINO exoskeleton at all orientations of joints 1, 2, and 3 of the exoskeleton to compensate for gravity.

Acknowledgements

I would like to thank Dr. Eric Wolbrecht for making my research possible with his continued support in all aspects of this project. Your willingness to spend time on brainstorming design ideas, troubleshooting problems, and editing and revising my thesis has been greatly appreciated. Your passion for both your research and as an educator is inspiring, and I can only hope to bring the same enthusiasm to my career in the future. I am also grateful for the opportunity to have been a TA for your classes for several semesters. The funding made a Master's degree possible for me and the experience I gained from helping students for those semesters was invaluable.

I would also like to thank Dr. Joel Perry, the PI of the BLUE SABINO project for the opportunity to work with you. I first started researching with you as an undergraduate senior on your Capstone project and your enthusiastic approach to tackling problems in rehabilitation design made joining BLUE SABINO a no-brainer for me. You have worked very hard on securing funding from NSF so that we can continue to push the boundary of rehabilitation robotics and I know I speak for everyone on the team when I say we are grateful.

A special thanks is due to my committee members; the previously mentioned Dr. Wolbrecht and Dr. Perry, along with Dr. Michael Maughan. Thank you for helping with the editing and revising of my thesis, for attending my defense, and for all of your guidance throughout this process.

Thank you to all of the members of the BLUE SABINO team; Chris Bitikofer, Rene Maura, Sabastian Rueda, Melissa Bogert, and Tony Branz. You all are incredible engineers, and more importantly, friends. You have helped me through tough classes and through many design challenges, and getting to work with you all each day has been an incredible privilege. I am so excited to see the amazing things you accomplish in your respective careers.

Finally, to all my friends, colleagues, and teachers throughout my life, you have helped shape me into the person I am today. The lessons I learned from you throughout my schooling have been too many to count, and I hope to make each of you proud with the work I do in the future

Dedication

I dedicate this work to my family.

To my parents, Lenny and Chris Hill. Thank you for your support and love through everything I have done. Words cannot describe how grateful I am for you each and every day. You have spent every bit of the last 25 years driving my siblings and I to sporting events, school trips, and countless other activities, all the while with smiles on your faces. You have sacrificed all of your free time and then some to allow us to chase our dreams. I am every bit of the man I am today because of you both, and I will always be thankful for the things you have taught me. I love you both.

To my older siblings, Chase, Adena, Rylan, Corbin, and TJ. You guys have always been there for me and I couldn't ask for better friends than you. I have learned countless lessons from you (even if some are what NOT to do), and I love you all.

To my twin brother, Preston. You have pushed me to be better in everything that I do. I can't imagine having tackled any of this without you. Your outlook on life is inspiring and I am very proud of the person that you have become. I look forward to seeing you take on the world and know you will do great things. You will always be my best friend, and I love you man!

Table of Contents

List of Tables

List of Figures

Chapter 1: Introduction

1.1 Stroke Background

Fifteen million people suffer a stroke each year, many of whom will survive with some form of impairment, making stroke one of the leading causes of adult disability in the world (Feigin et al., 2014). A stroke occurs when blood flow to some area of the brain is restricted or cut off due to a clot or other blockage. With this lack of blood flow, brain cells lack the oxygen they need to survive and begin to die. When these cells die, the functions, which can include memory and muscle control, controlled by that portion of the brain are lost. These losses often lead to impairment in movement and speech, among other things. Extensive research has demonstrated the efficacy of rehabilitation training to improve arm function after stroke (Langhorne et al., 2011), particularly soon after the stroke occurs (Kwakkel et al., 2004). In the three months that follow a stroke, the effectiveness of rehabilitation to recover these losses in function have shown to be higher than in the months that follow. Other research suggests that assessment of neuromuscular impairments caused by stroke may help in the selection of targeted therapy interventions to improve outcomes (Colombo et al., 2005). While this research is encouraging for the long-term health of stroke survivors, it also highlights the need for proper access to assessment and rehabilitation early and often after a stroke occurs.

In the United States the large number of stroke survivors have significantly strained the current healthcare system, incurring huge direct and indirect costs and taxing the limited pool of healthcare professionals (American Heart Association, 2019). This problem is projected to grow as the population continues to age (Ortman et al., 2014) and advances in post-stroke medicine lead to lower stroke mortality rates (Yang et al., 2006). Both factors lead to a higher number of survivors with impairment that require rehabilitation.

Robotic devices have the potential to meet the growing need for cost-effective assessment and rehabilitation of stroke patients. Research is ongoing, but previous review literature (Norouzi-Gheidari et al., 2012), (Tran et al., 2018), (Prange et al., 2006), has demonstrated that robotic devices are able to assess and quantify impairment in ways not otherwise possible. Furthermore, robotic devices for post-stroke movement therapy have

demonstrated promising efficacy, with results equaling and, in some cases, marginally exceeding conventional therapy in dosage-matched comparisons (Prange et al., 2006),(Norouzi-Gheidari et al., 2012). Some robotic devices have been shown to be capable of both studying and administering movement therapy and performing assessment. An example of such a device is the BiLateral Upper-extremity Exoskeleton for Simultaneous Assessment of Biomechanical and Neuromuscular Output (BLUE SABINO) (Perry et al., 2019), which is currently under development at the University of Idaho and is specifically designed for both post-stroke assessment and rehabilitation.

1.2 BLUE SABINO Background

BLUE SABINO is an exoskeleton device designed to assist in the assessment and rehabilitation of motor deficiencies in the upper limbs of stroke patients. The goal of the project is to create a system to aid in the assessment of the range of motion, neuromuscular output, force production capabilities, and abnormal synergies in the upper limbs of stroke patients. The system will simultaneously record output from force/torque sensors and electroencephalogram (EEG) and electromyography (EMG) sensors during assessment and rehabilitative therapy. These sensor readings combined with kinematic feedback from the exoskeleton motors create a broad, quantitative description for assessment of impairment due to stroke. Furthermore, this assessment data is collected and available for real-time control, allowing for the implementation and evaluation of novel experiments and therapy protocols designed to increase our understanding of impairment and recovery after stroke. The knowledge gained from the system should provide medical professionals the ability to properly prescribe targeted therapies to improve patients' recovery after suffering a stroke.

A rendering of the current solid-model design of the BLUE SABINO upper-extremity exoskeleton is shown in Figure 1.1. It is an extension of the EXO-UL series exoskeletons designed by Rosen et al., and in particular, the EXO-UL7 (or CADEN 7) and the EXO-UL8. The EXO-UL7 had a light-weight design that allowed for near full range of motion of the upper extremity allowing for common movements including many activities-of-daily living (ADL) tasks (Simkins et al., 2013). The EXO-UL8 was the first of this series of exoskeletons to eliminate much of the cable routing used for remote actuation, and instead place Harmonic Drive motors at each joint (Shen et al., 2018). The addition of these motors led to increased

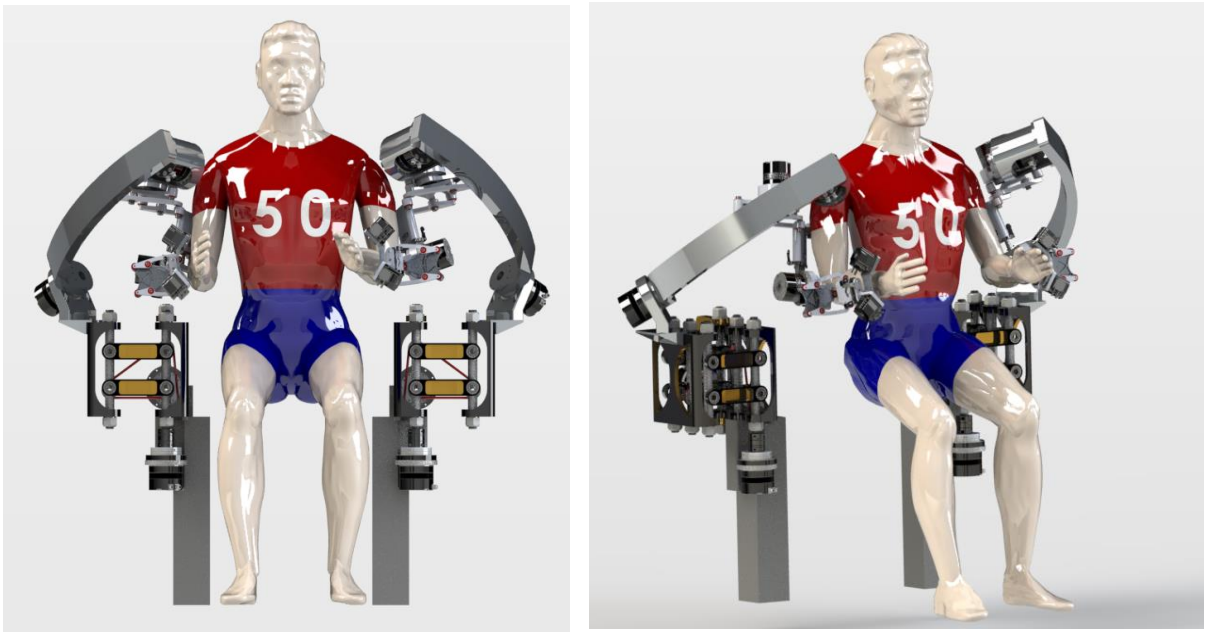

Figure 1.1. Rendering of the solid-model of the current BLUE SABINO exoskeleton design. Image reprinted from Trimble (2016).

positional accuracy and helped alleviate the issues of prematurely breaking cables and related hardware. The addition of these motors, however, also resulted in a large increase in the weight of the exoskeleton. This raised the strength and stiffness required for each link, and the torque requirements for each joint, which now must carry the additional load of downstream motors. The design of BLUE SABINO keeps many of the features of the EXO-UL8, including the use of Harmonic drive motors, while implementing some additions and improvements to the overall design.

One of the central goals of the BLUE SABINO project is to add an additional 2 degrees of freedom (2 DOFs) that will allow for movement of the clavicular joint in the shoulder and enable scapulohumeral rhythm, improving the alignment of the exoskeleton to the user and allowing for normal shoulder movement during use. Most previous robotic exoskeleton devices simplify the shoulder as a fixed spherical joint. In reality, however, the location of the shoulder joint translates vertically (elevation and depression) and horizontally (protraction and retraction) during regular use of the arm. Figure 1.2 shows the joints of the human shoulder (Perry et al., 2018). A study of numerous common ADL tasks was conducted to determine typical shoulder displacement magnitudes during normal arm use (Bitikofer et al., 2019). To do this, motion-capture data from the ADL tasks was analyzed

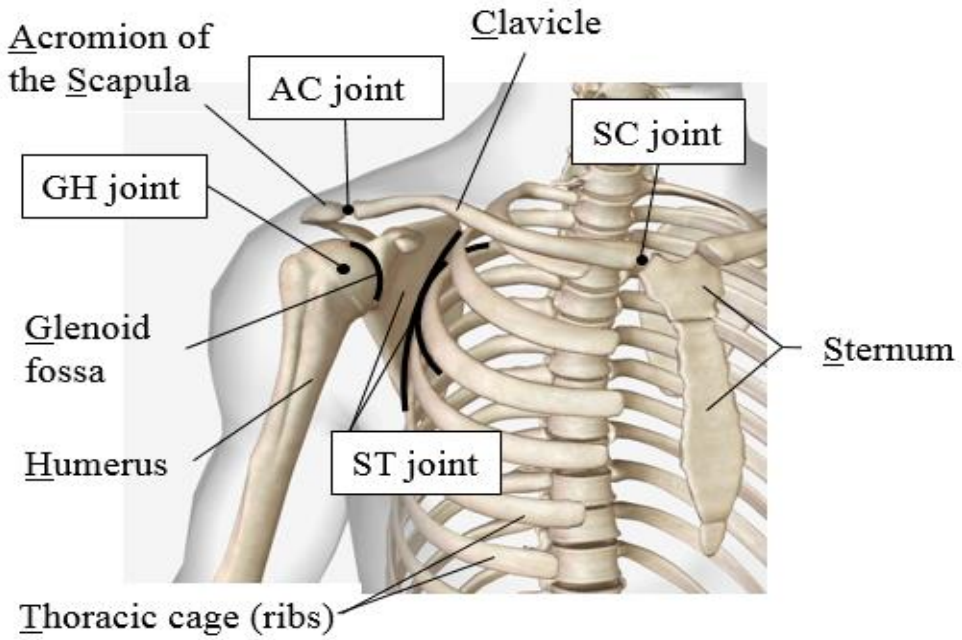

Figure 1.2. The joints of the human shoulder. Motion of the shoulder and arm are accomplished through the combined motions of the sternum/clavicle (SC), acromion/clavicle (AC), and glenoid/humerus (GH) joints. Image reprinted from Perry et al. (2018).

and the magnitude of shoulder displacement calculated relative to the initial position. Results from the study are given in Figure 1.3, which shows histograms of time spent at specific shoulder displacement magnitudes for four categories of ADL tasks.

It is clear in Figure 1.3 that displacements of the location of the center of the shoulder of 5-10+ cm are very common during typical ADL tasks. Thus, simplifying the shoulder to a spherical joint limits the natural motion patterns of a patient and can cause misalignment between the exoskeleton and shoulder joint. For these reasons, several previous research groups have included additional DOFs to account for these movements. These robotic exoskeletons, along with some that don't allow shoulder displacement, are described in the following section that details the current state of the art in upper-extremity exoskeletons.

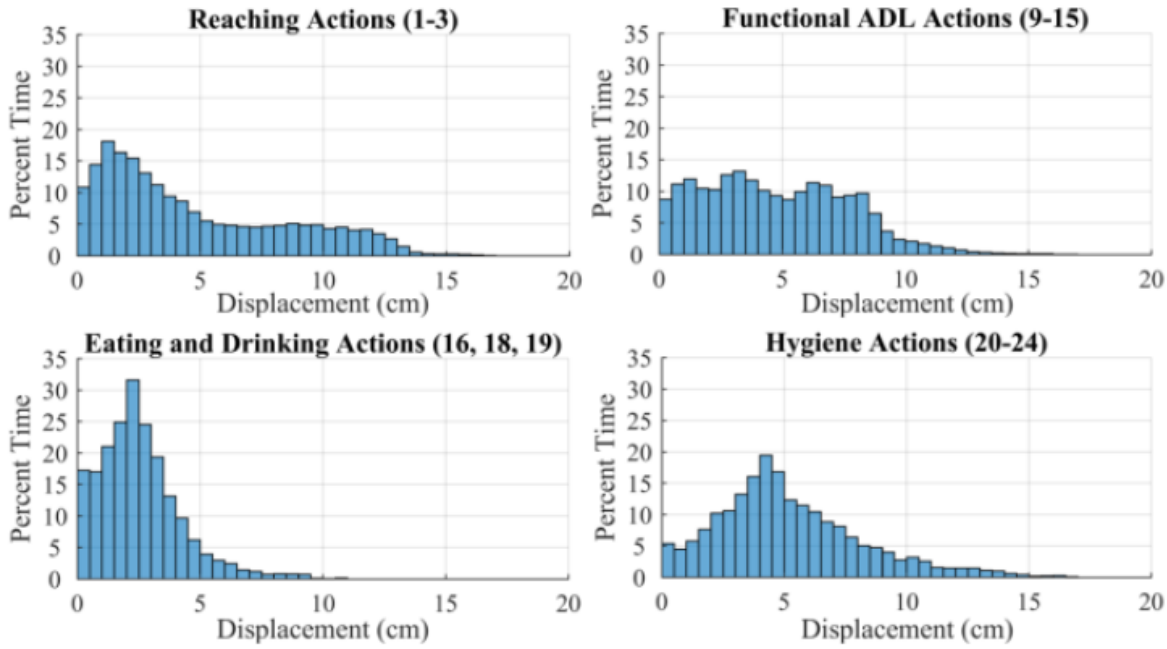

Figure 1.3. Histograms of time spent at specific shoulder displacement magnitudes. As an example of how to interpret these histograms, the distribution shown in the lower-left plot indicates that the shoulder is displaced approximately 2 cm for 30% of the time during eating and drinking actions. All four of these distributions were found from an analysis of motion-captured data from numerous activities-of-daily-living (ADL) tasks. Image reprinted from Bitikofer et al. (2019).

1.3 Upper-Limb Exoskeleton State of the Art

Numerous upper-extremity robotic devices have been designed for post-stroke rehabilitation and/or other human-robot tasks. Most of these exoskeletons (Rahman et al., 1995), (Mistry et al., 2005), simplify the shoulder joint as a 3-DOF spherical joint, typically constructed with 3 revolute joints with axes intersecting at the center of the shoulder joint. This kinematic design neglects the motion of the scapulothoracic (ST) and sternoclavicular (SC) joints. However, the fixed spherical joint has the advantage of reduced complexity, weight, and cost for motors and components that would be needed for actuating these neglected motions. The first three exoskeleton devices presented in the paragraphs that follow simplify the shoulder joint to a 3-DOF spherical joint; the remaining exoskeletons discussed in this section include at least 4 DOFs at the shoulder joint to accommodate motions of the shoulder complex.

ExoRob is a 7-DOF exoskeleton device (with 3 actuated revolute joints mimicking a 3-DOF spherical joint at the shoulder, along with actuated joints for elbow flexion/extension, forearm pronation/supination, wrist radial/ulnar deviation, and wrist flexion/extension (Rahman et al., 2010). The device is actuated with DC motors and designed to assist disabled

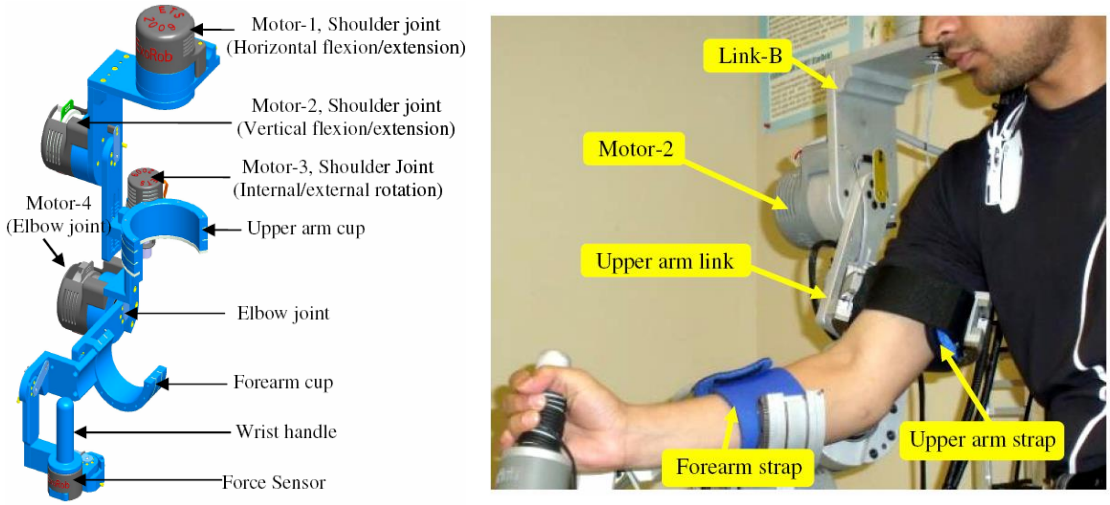

Figure 1.4. The ExoRob robotic exoskeleton. The left side shows a solid model of the exoskeleton with a description of several components and the right side shows the device in use. Image reprinted from Rahman et al., (2010).

people with impaired upper-limb function. The 7-DOF ExoRob design (Figure 1.4) does not include actuation for elevation/depression and protraction/retraction of the shoulder joint. The device is mounted rigidly above the shoulder of the patient, and the location of the shoulder joint cannot move during use without misalignment between the patient and the exoskeleton.

The Sarcos Master Arm (Figure 1.5) is another 7-DOF robotic exoskeleton device designed for interaction with the human arm. This device, developed by Sarcos, Inc. includes a 3-DOF spherical joint for the shoulder, one for elbow flexion/extension, forearm pronation/supination, wrist flexion/extension, and wrist radial/ulnar deviation (Mistry et al., 2005). The exoskeleton is hydraulically actuated and controlled using feedback from potentiometers and force sensors at each joint. Like ExoRob, the Sarcos Master Arm simplifies the shoulder as a fixed-center spherical joint, neglecting elevation/depression and protraction/retraction of the shoulder joint. Once again, the device is mounted rigidly around the

Figure 1.5. The Sarcos Master Arm. Image reprinted from Mistry et al. (2005).

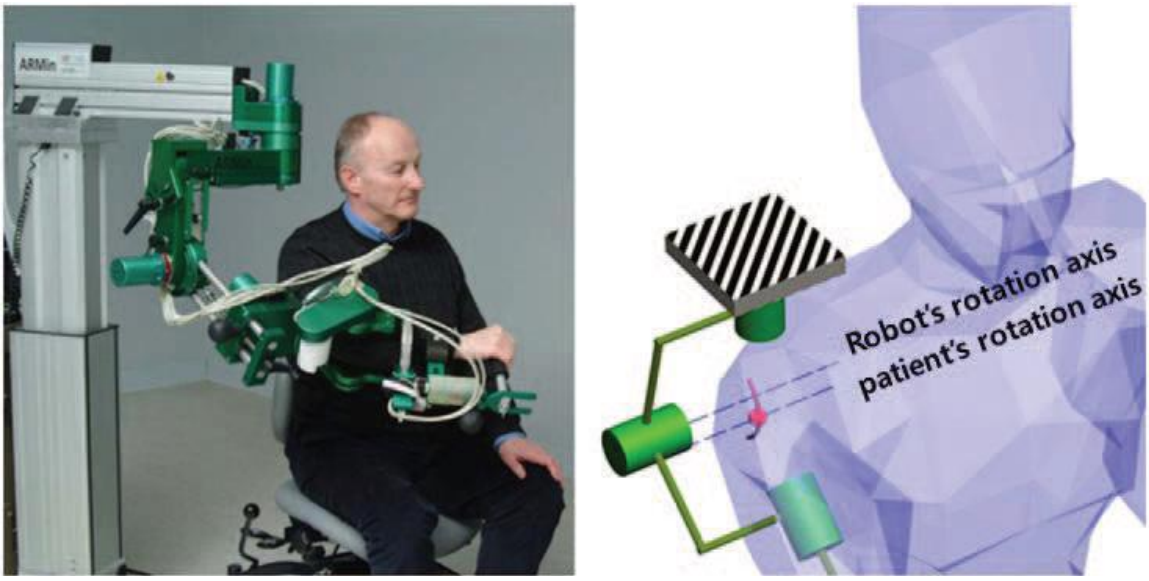

Figure 1.6. The robotic exoskeleton ARMin III. The left side shows ARMin III in use and the right side shows the approximation used for the shoulder joint of the exoskeleton. Image reprinted from Guidali et al. (2009).

shoulder of the patient and the location of the shoulder of the patient cannot move during its use or misalignment can occur.

The ARMin III (Figure 1.6) is a 6-DOF robotic exoskeleton device that also simplifies the shoulder as a 3-DOF spherical joint comprised of three revolute joints. In addition to the 3-DOF at the shoulder, the device also allows elbow flexion/extension, forearm pronation/supination, and wrist flexion/extension, all actuated by DC motors (Guidali et al., 2009). The goal of the device is to assess abnormal muscle synergies in patients following a stroke and to administer and study movement therapy. While the device can be adjusted vertically for patient height, the location of the shoulder joint is not actuated during use. Because of this, once again, misalignment of the shoulder joint can occur if the location of the patient's shoulder joint moves.

The first device presented here that includes additional DOF at the shoulder joint is IntelliArm (Figure 1.7). IntelliArm is a 9-DOF (seven active, two passive) exoskeleton that includes four active and two passive joints at the shoulder, two active DOF at the elbow, and one active DOF at the wrist, along with an active joint at the hand for opening and closing tasks (Park et al., 2008). In particular, the exoskeleton is intended to diagnose abnormal muscular synergies through the ability to isolate individual joints during use. The device can also be used for administering movement therapy. The passive prismatic joints at the

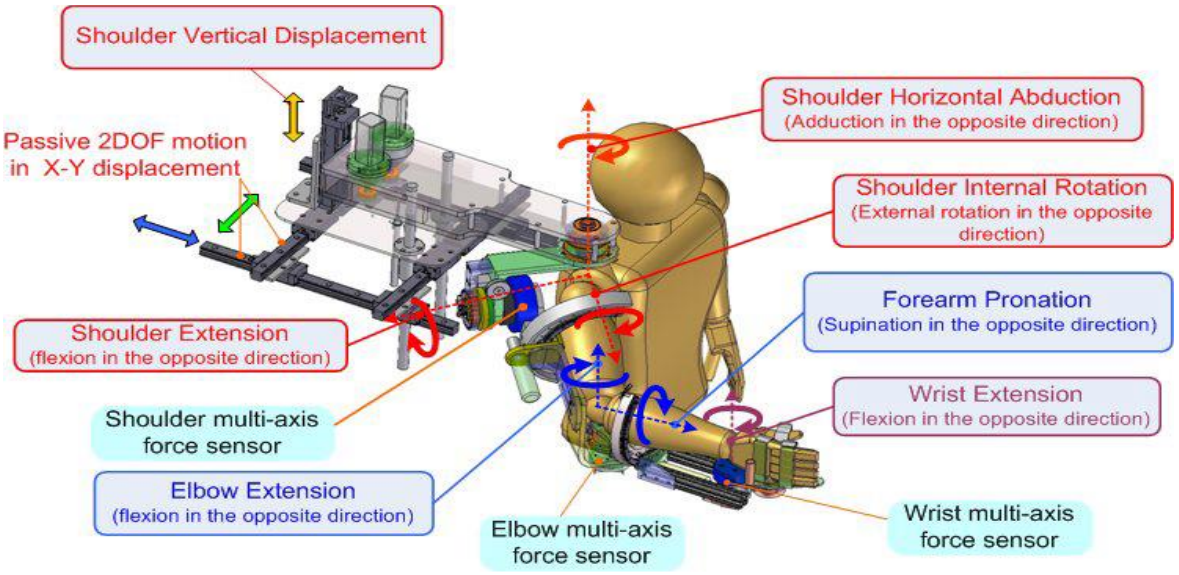

Figure 1.7. The IntelliArm robotic exoskeleton and descriptions of several of the main features of the design. Image reprinted from Park et al. (2008).

shoulder allow horizontal (X-Y) translation of the shoulder joint with linear guide rails. Vertical translation of the shoulder is also accounted for in a similar, active, linear rail. The weight of the device is balanced actively in a vertical actuator, which must always lift the weight of the device and allow patient movement.

MEDARM (Figure 1.8) is a 6-DOF robotic exoskeleton device that actuates 5 DOF at the shoulder joint, three for the shoulder joint itself and two for elevation/depression and

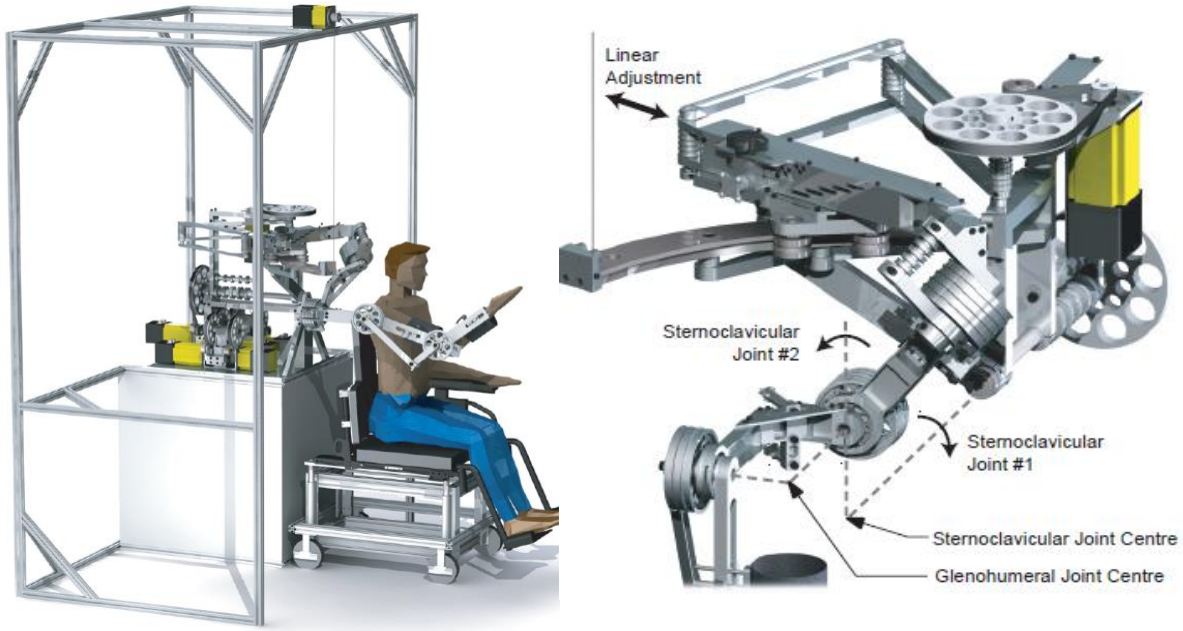

Figure 1.8. The MEDARM robotic exoskeleton. The left side shows the entire device, while the right side highlights the mechanism used for shoulder articulation. Image reprinted from Ball et al. (2007).

protraction/retraction of the shoulder, in addition to flexion/extension of the elbow (Ball et al., 2007). The goal of this device is to allow rehabilitation of the shoulder complex through more accurate modeling of the shoulder girdle. MEDARM is a remotely actuated, cable-driven robotic exoskeleton, which allows the electric motors to be located at the base of the device and enables a lightweight design. The translation of the shoulder is accomplished with a rotary joint to provide elevation and depression of the shoulder and a curved track system for protraction and retraction of the shoulder joint. The inclusion of additional degrees of freedom for motion of the shoulder joint has led to a larger, more complicated design. A large frame is included to allow gravity compensation of the device using a motorized vertical cabling system shown in Figure 1.8..

Finally, the Harmony exoskeleton (Figure 1.9) is a 7-DOF exoskeleton with 5 DOFs at the shoulder, and 1 DOF at each of the elbow and wrist mechanisms. Harmony was designed to assist in administering rehabilitation therapy while allowing users full range of motion of the shoulder joint during movements (Kim and Deshpande, 2017). It is powered by series-elastic actuators modified with a brushless DC motor. The exoskeleton includes a parallel four-bar mechanism and a single revolute joint for actuating both elevation/depression and protraction/retraction of the shoulder during use. The gravity

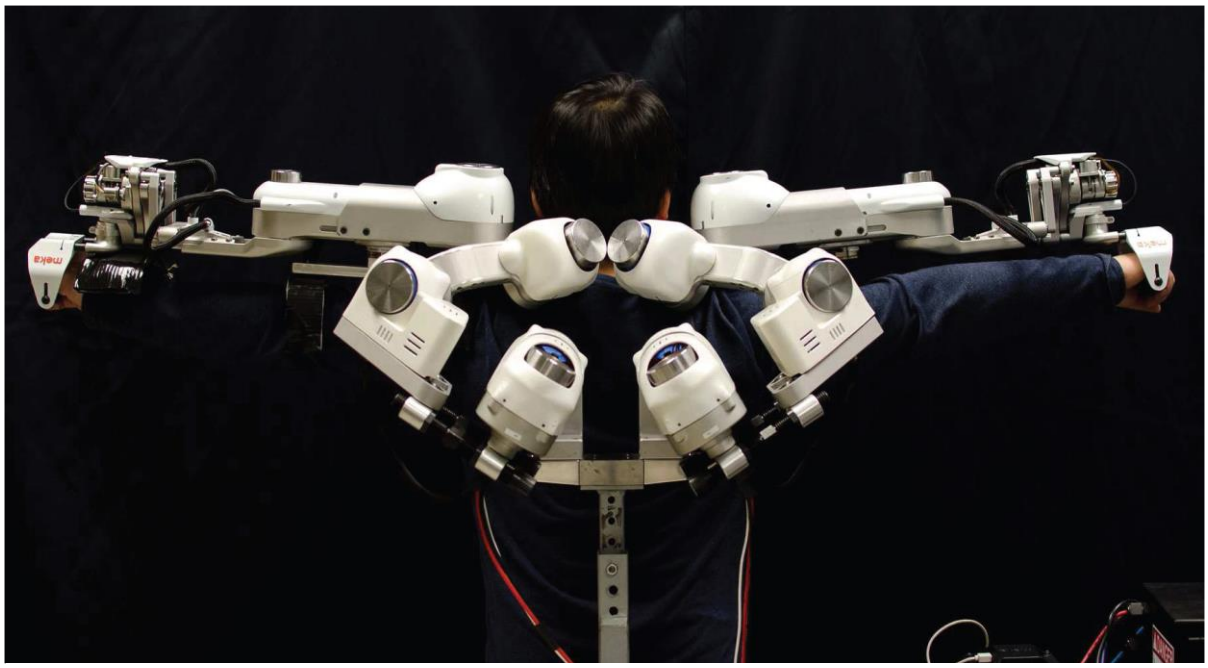

Figure 1.9. The Harmony exoskeleton during use. Image reprinted from Kim and Deshpande (2017).

balancing in the device is done actively in the motors of the exoskeleton with no other balancing present.

The robotic exoskeletons discussed in this section present unique design solutions for assisting in rehabilitation and assessment of upper-extremity impairment in people who have suffered a stroke. Many of these designs omit joints for the elevation/depression and protraction/retraction of the shoulder joint. Including these clavicular motions presents several challenges to design, which several of the previously described devices attempted to address. The current design of BLUE SABINO also includes additional DOFs for these clavicular motions along the accompanying challenges this inclusion presents. One such challenge, providing gravity compensation to a joint that moves as a result of this inclusion, is the focus of this thesis.

1.4 Motivation for Gravity Balancing in BLUE SABINO

The BLUE SABINO exoskeleton includes a 2-DOF clavicular joint mechanism that was not part of its parent exoskeleton, the EXO-UL8. Actuation of the vertical component of clavicular motion, elevation and depression of the shoulder joint, necessitates vertical motion of the entire exoskeleton. This means that actuation of this joint includes supporting the weight of the downstream exoskeleton and the arm of the subject. These weight-supporting forces, i.e. gravity balancing forces, create an offset, or bias, in the torques required from the motor. That is, in addition to torques required for arm motion, the motors must always provide the torque to counteract the weight of the robot and arm. This requires larger motors to supply the needed torque since a significant portion of the motor’s working range is utilized to offset this torque bias.

Figure 1.10 shows the BLUE SABINO exoskeleton and the location of joints 1-6. Joint 1 allows for protraction/retraction of the shoulder joint during clavicular motion while joint 2 allows for elevation/depression of the same joint. Joints 3, 4, and 5 create the spherical joint at the shoulder, and joint 6 accounts for elbow flexion/extension. To determine the required torque distributions of each actuator (located at each joint), a kinematic analysis of the BLUE SABINO exoskeleton during ADL tasks was conducted. The analysis used motion capture data collected from a healthy patient performing several ADL tasks independently (without being connected to an exoskeleton). These motions were then considered as desired trajectories for the joints of BLUE SABINO. Inverse kinematics and dynamic simulation allowed the mapping of these ADL tasks to movements and torques at the joints of BLUE SABINO (Bitikofer, 2018). Figure 1.11. shows the torque distributions at joints 1-6 of BLUE SABINO during these typical ADLs. This figure shows that the torque distributions of joints 1, 4, 5, and 6 are centered near zero. This means that during motions similar to the ADLs, the motors will spend nearly equal time producing positive and negative

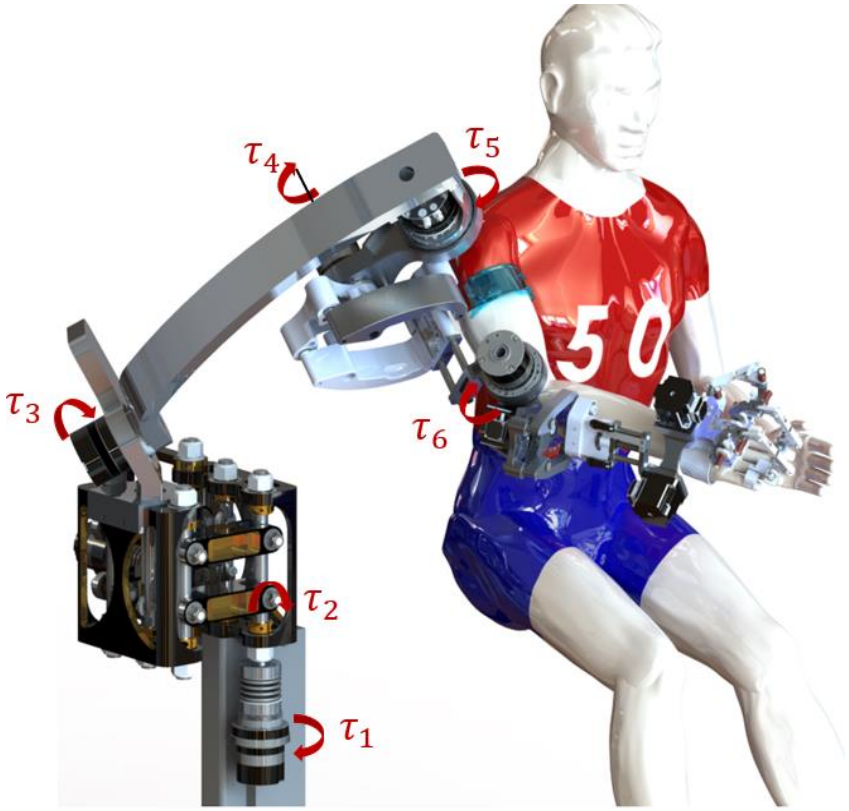

Figure 1.10 Rendering of the BLUE SABINO exoskeleton. Joints 1 through 6 are labeled τ_1 through τ_6 with positive directions indicated by arrows.

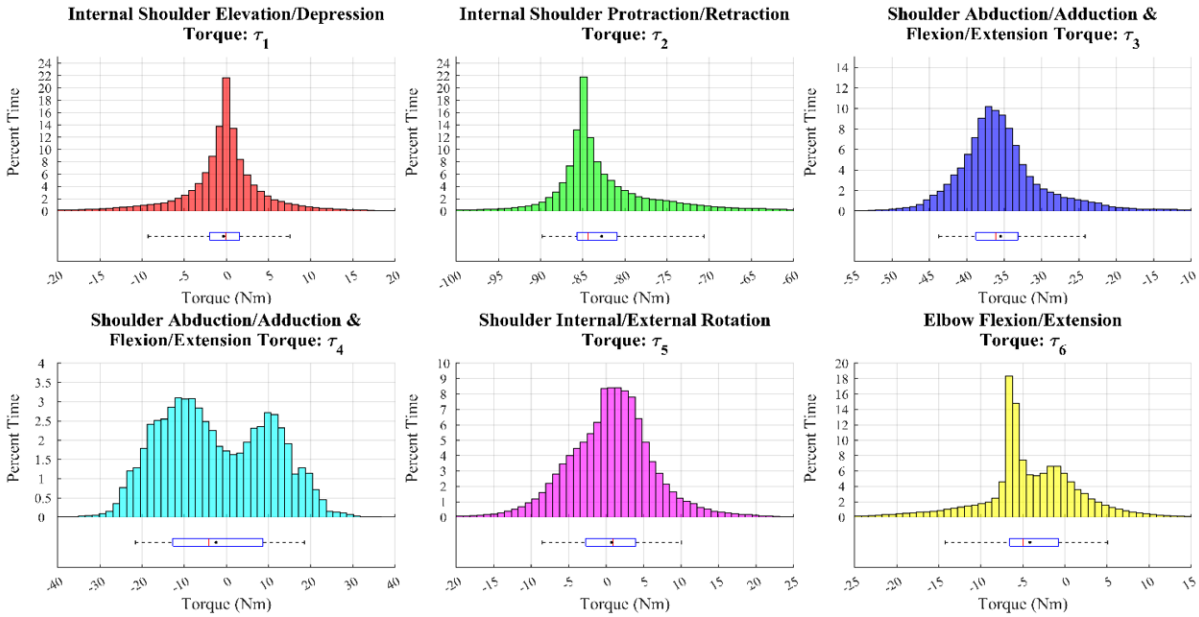

Figure 1.11. Torque distributions during representative ADL motions. Histograms for percent time at specific actuator torques are shown for actuators 1:6 of the BLUE SABINO exoskeleton. Image reprinted from Bitikofer (2018).

torques of similar magnitudes. In the case of joints 2 and 3, however, the centers of their respective distributions are clearly shifted negatively.

The nature of the design of the exoskeleton from Figure 1.10 means the weight of the robot and arm create large torques on joints 2 and 3 in typical arm configurations. This is evident in the torque distributions of joints 2 and 3 shown in Figure 1.11., which are centered around -83 N-m and -35 N-m, respectively. This makes these joints great candidates for the addition of a gravity-balancing mechanism, as shifting the center of these distributions closer to zero with a passive elastic element could lead to a significant reduction in the size of the motors needed for actuation.

1.5 Joint Balancing with Passive Elements

Joint balancing is not a new concept in exoskeleton devices. Counteracting the weight of the device against gravitational forces independent of orientation allows for more effective use of exoskeleton devices as the counteracted weight no longer affects patient movement. While some of the devices mentioned in section 1.3 have compensated for weight through larger active mechanisms or rough approximations of joints, few allow nearly full range of motion to the user while accomplishing gravity compensation. This section will cover passive balancing devices and several exoskeletons that utilize them.

Many solutions have been found for achieving passive gravity equilibrium in previously developed devices. Counterweighting, or balancing with a mass, is one method that has been used extensively. It involves applying a mass at the end of a moment arm to counter the weight at the other end. This is a simple solution but requires a lot of space or a large counterweighting mass. Given the relatively small space an exoskeleton encompasses and the added inertia to the system from potentially large masses, counterweighting does not represent a feasible solution to the gravity balancing of exoskeleton joints.

Another method often used to achieve gravity equilibrium is using springs. Springs have been used heavily in static balancing applications. One such application is the zero-free-length spring mechanism, in which a spring is attached to a link at one end and to a fixed position directly in line with the rotation axis of the link on the other. An image of this is shown in Figure 1.12. (Herder, 2001). The use of a zero-free-length spring in this application reduces the summation of moments about the pivot point to the following:

$$mgr_m = rka \tag{1.1}$$

where m is the mass, g is gravitational acceleration, r_m is the distance from the pivot to the center of mass, k is the spring constant, and a is the distance from the pivot to the fixed end

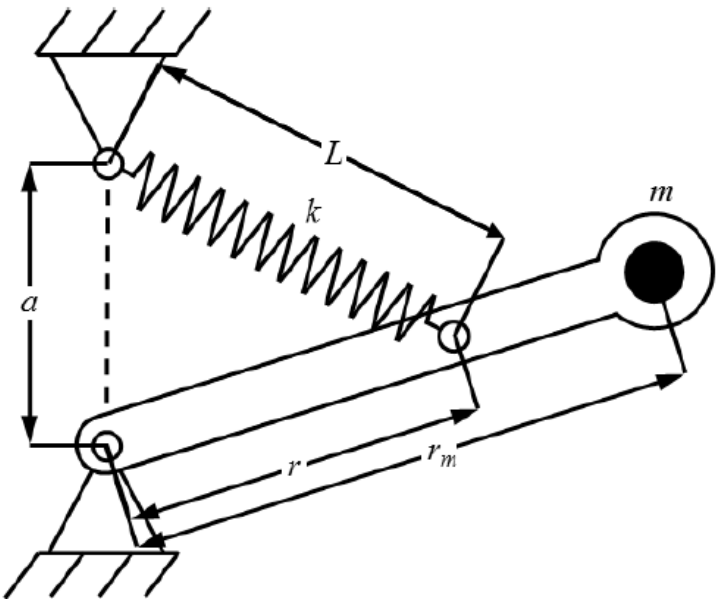

Figure 1.12. A typical zero-free-length spring gravity compensation mechanism. The mechanism uses is a zero-free-length spring to produce constant vertical force at any angle. Image reprinted from Herder (2001).

of the spring (Herder, 2001). Careful selection of r,k, and a can lead to equilibrium for any combination of mass (m) and distance to the center of gravity (r_m).

Most springs available off-the-shelf, however, have a zero-free-length of 70-80% of their initial length, not zero like is required for use in the mechanism from Figure 1.12. (Herder, 2001). For that reason, modifications to the concept from Figure 1.12. have been made to replace zero-free-length springs with linear springs. One such modification is to use pulleys to hide the initial stretching of the spring somewhere out of line with the connection between the link and fixed position. In this orientation, initial tension can be added to the spring while keeping the attachment length (L) the same, essentially creating a zero-free-length spring at that position. Figure 1.13. shows this application. This modification allows for the use of linear off-the-shelf springs in the application of gravity balancing while still maintaining gravity equilibrium at all positions.

One such device that uses this concept is the WREX (Wilmington robotic exoskeleton) (Rahman et al., 2004), (Rahman et al., 2006). In a recent design, gravity balancing is accomplished using rubber bands. The concept is applied at two separate joints in the device (upper-arm, and lower-arm) shown in Figure 1.14.. The springs are stretched as the joint angle changes, and the supplied force balances the gravity of the device and arm of the patient. To produce larger forces, the number of rubber bands utilized must simply be

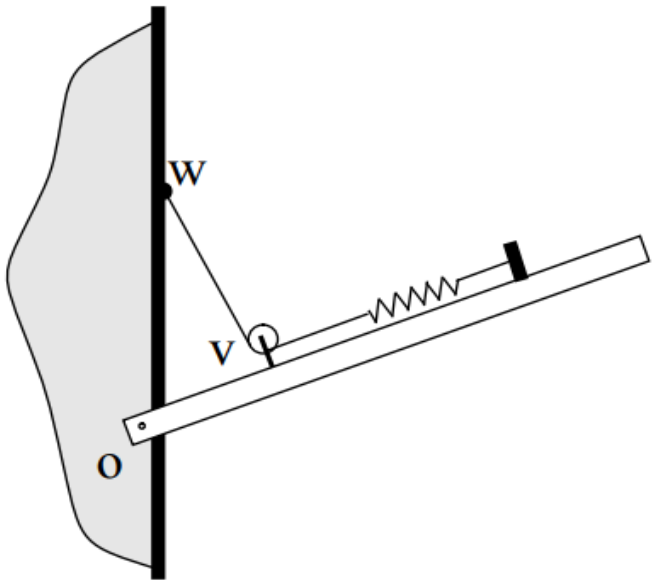

Figure 1.13. A typical modification made to the simple gravity balancing mechanism to utilize a linear spring instead of a “zero-free length” spring. Image reprinted from Rahman et al. (1995).

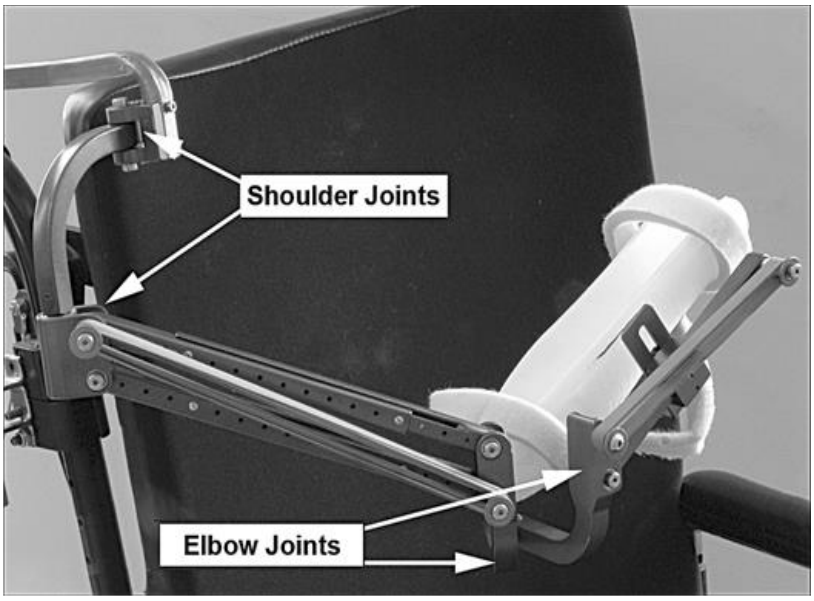

Figure 1.14. The WREX exoskeleton with spring balancing at the shoulder and elbow joints. Image reprinted from Rahman et al. (2006).

increased until the desired force values are created. This concept, while simple for this implementation, provides much smaller torques at the joints of the exoskeleton than are required in the BLUE SABINO exoskeleton.

Joint 2 of BLUE SABINO is also designed to utilize the zero-free-length spring concept, specifically utilizing the modified version with linear springs from Figure 1.13.. Joints 1 and 2 are part of PRISM (Parallel Rotating mechanism for the Inclusion of Scapulothoracic Motion), a spatial 2-DOF parallel mechanism which allows scapulothoracic motion of the shoulder joint. The design of PRISM includes a cable connected to a linear spring using pulleys to provide a gravity-balancing torque to joint 2. It is designed under the assumption that the length of the cable for routing does not change (i.e. the linear spring length does not change) during rotation of joints 1 and 2 of the exoskeleton (see Figure 1.15). This assumption, however, is not entirely accurate, as the cable length changes slightly as joint 2 rotates. For this reason, a non-constant force may be created from the mechanism because of the use of the linear spring. Additionally, the nature of joint 2 as a translation mechanism works well with the zero-free-length spring concept, while the motion required to actuate joint 3 does not.

Many other methods for statically balancing joints exist as well, including other applications of linear springs (Lee and Seo, 2017), (Chung et al., 2016) among others. The

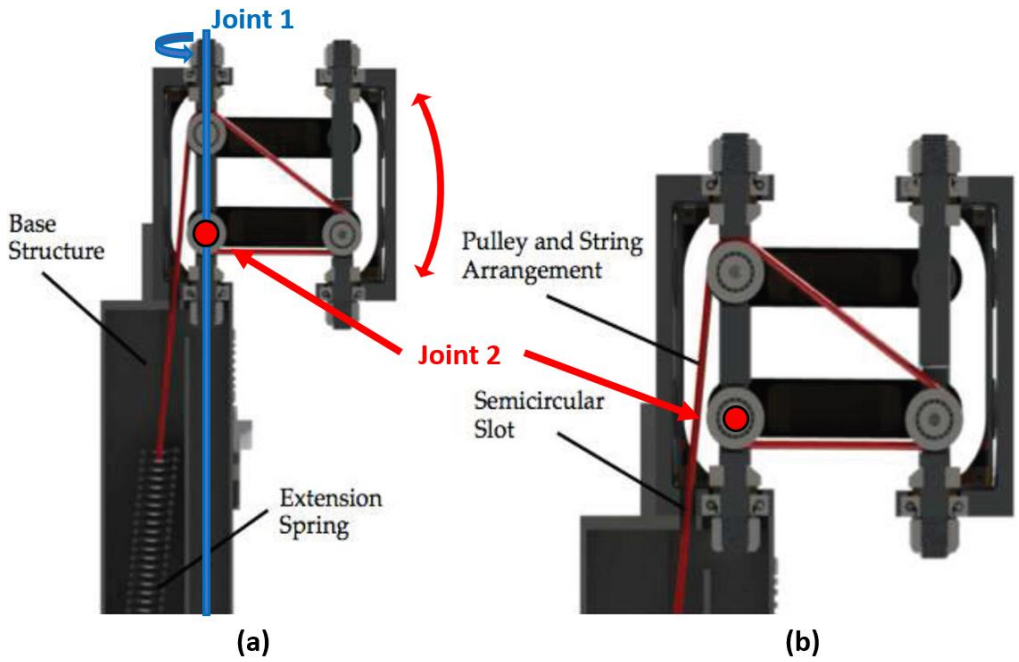

Figure 1.15. a) Existing balancing mechanism using a linear spring for joint 2. b.) Enlarged view of the cable-pulley assembly in joint 2. Image adapted from Trimble (2016).

desired torques in joints 2 and 3 of BLUE SABINO, however, are much larger than those in most of these devices. These significantly larger torques create challenges in these designs because the springs (rubber, linear, or other) must be much larger and, in turn, weigh much more and occupy much more space. For these reasons, an alternative method to achieve a constant gravity-balancing torque at joint 3 from the methods presented in this section is required.

In summary, the design of BLUE SABINO allows movement of the shoulder joint, which requires the use of larger motors than desired. In addition, the large torques required during normal use of the BLUE SABINO exoskeleton make the use of passive joint balancing as it is implemented in other smaller devices very difficult. Finally, the method utilized for joint 2 in BLUE SABINO represents a possibility for accomplishing this balancing, but limited space in the PRISM mechanism and the rotating nature of joint 3 necessitates the investigation of another mechanism to accomplish this gravity balancing. Creation of a passive constant-torque mechanism for gravity compensation of joint 3 in a way that requires minimal change to PRISM is desired. This passive element coupled with the motor at joint 3 should allow for complete gravity compensation of the joint at all orientations.

1.6 Constant Force Springs

One method of delivering a constant passive torque is with constant-force springs, which are designed to deliver a near-constant force over a large displacement range. Supplying a constant force at a constant moment arm to a motor creates a constant torque that could be used for gravity balancing.

Figure 1.16. Typical constant-force spring.

A constant-force spring is usually a strip of spring steel tightly wound on a mounting drum (see Figure 1.16). As a tensile force is applied to the end of the spring, it unravels. Unlike a linear spring, in which force generation is proportional to displacement, a constant-force spring is designed to supply a constant force throughout its displacement range. Figure 1.17 (a) shows the general theory of a constant force spring vs. a linear coil spring. `

Although a constant-force spring is designed to produce a constant force throughout its displacement, a study by Atsumi Ohtsuki and Shigemichi Ohshima (Ohtsuki et al., 2001) showed that there is a relationship between force and displacement, and that it can be characterized generally by a curve like the one shown in Figure 1.17 (a). Their findings showed that at small displacements (ratio of displacement to spring radius, x/R below 5), the

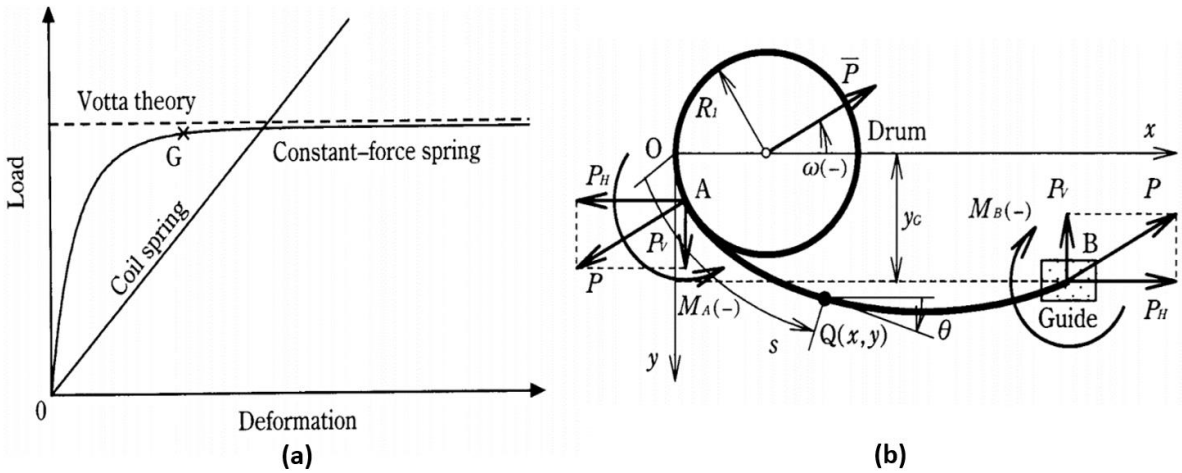

Figure 1.17. (a): Typical force vs. deformation curve for constant-force springs and linear springs. (b): Typical free-body diagram of a constant-force spring during displacement (x). Images reprinted from Ohtsuki et al. (2001).

force profile was not constant. At larger displacements (x/R above 8), the force profiles become much more constant. A typical free-body diagram of a constant-force spring is shown in Figure 1.17 (b). The forces P_V and P_H make up the components of the overall force P at the end of the spring. P_V is the force perpendicular to the displacement direction, and is wasted, while P_H is the measured force output of the spring. As the displacement distance (x) increases, the component P_V approaches zero. This results in growing measured force in the direction of P_H until P and P_H are nearly equal. At this point, the measured force (P_H) becomes very consistent and the force profile evens out.

These results suggest that constant-force springs represent a viable solution to providing a constant torque so long as the initial displacement of the spring is kept above a minimum threshhold. Chapter 2 of this thesis will cover the testing and validation of this theory, and the investigation of the force profile and friction characteristics of constant-force springs. Once feasability has been determined, Chapter 3 will present the design of a constant-torque mechanism to gravity balance joint 3 of the BLUE SABINO exoskeleton and implementation of the mechanism into the existing design of PRISM.

Chapter 2: Force Profile and Friction Testing of Constant-Force Springs

This chapter describes the experiments conducted to determine the force and friction characteristics of constant-force springs. The constraints for the experiments will first be presented in sections 2.1-2.3 followed by the presentation of the results and discussion of the findings in sections 2.4-2.6.

2.1 Experimental Constraints from BLUE SABINO

A simple way to create a constant torque at a joint with coiled springs can be done most simply with constant-torque springs. These springs are designed to provide a constant torque to an axis at any angle of rotation of the spring and are used in applications like seatbelts and drawer-closing mechanisms. However, constant-torque springs are more often used in very low-torque applications (0.01-5 N-m) than higher-torque applications like the 35N-m range required for joint 3 of BLUE SABINO. Much of this is because constant-torque springs are typically designed to work over a range of 10-20 full rotations. In the application of exoskeleton gravity-balancing, however, the range of rotation is normally less than 1 full

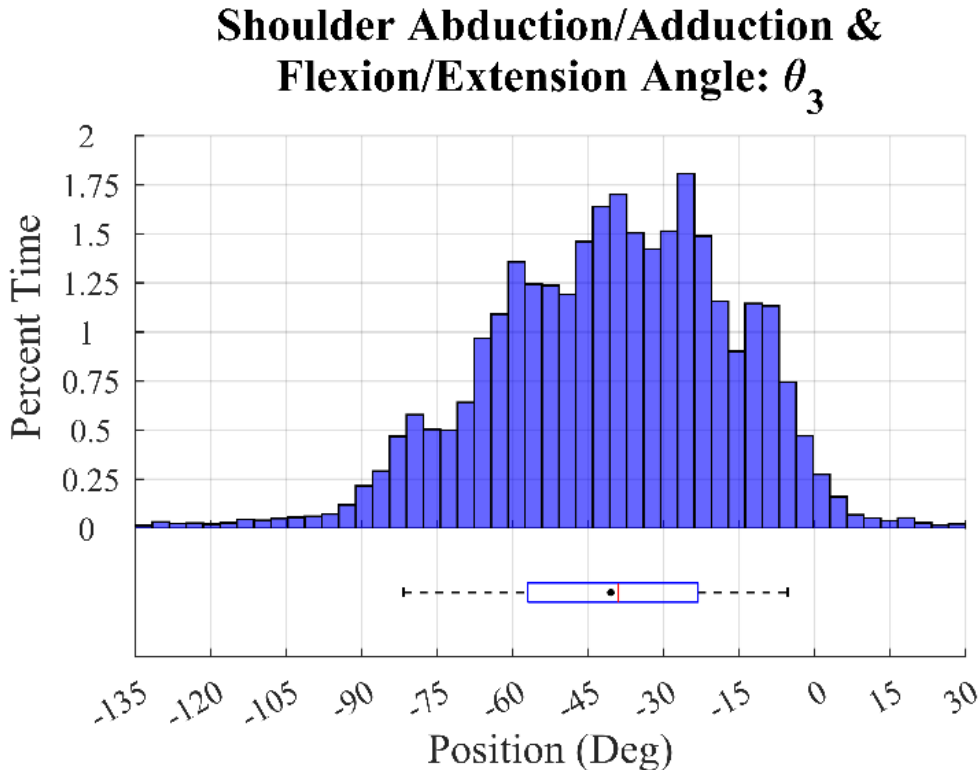

Figure 2.1. Typical position of the actuator at joint 3 of the BLUE SABINO exoskeleton. X-axis is the angle of joint 3 (in degrees) and the y axis is % time spent there during selected ADL tasks. Image reprinted from Bitikofer (2018).

rotation. For joint 3 of the BLUE SABINO exoskeleton, 160 degrees of rotation is sufficient. This is clear in Figure 2.1., which shows the typical time spent at the given angles for the joint.

Since less than half of a rotation is needed for the working range of joint 3 of the BLUE SABINO exoskeleton, constant-force springs were found to be a more appropriate design choice than constant-torque springs since the forces they create can be applied at a larger diameter to create larger torques. In addition, a working range of 180 degrees for experimental testing was chosen to properly encompass the range of joint 3.

2.2 Spring Configurations and Mounting

As mentioned previously, a constant torque can be achieved by connecting the constant-force spring to a simple cable and cam mechanism (Figure 2.2). If more than one spring is required, multiple mounting options are possible including back-to-back springs and springs wrapped together in parallel (Figure 2.3). Since the required torque value is relatively large (35 N-m for joint 3), using multiple springs and one or both of these mounting methods

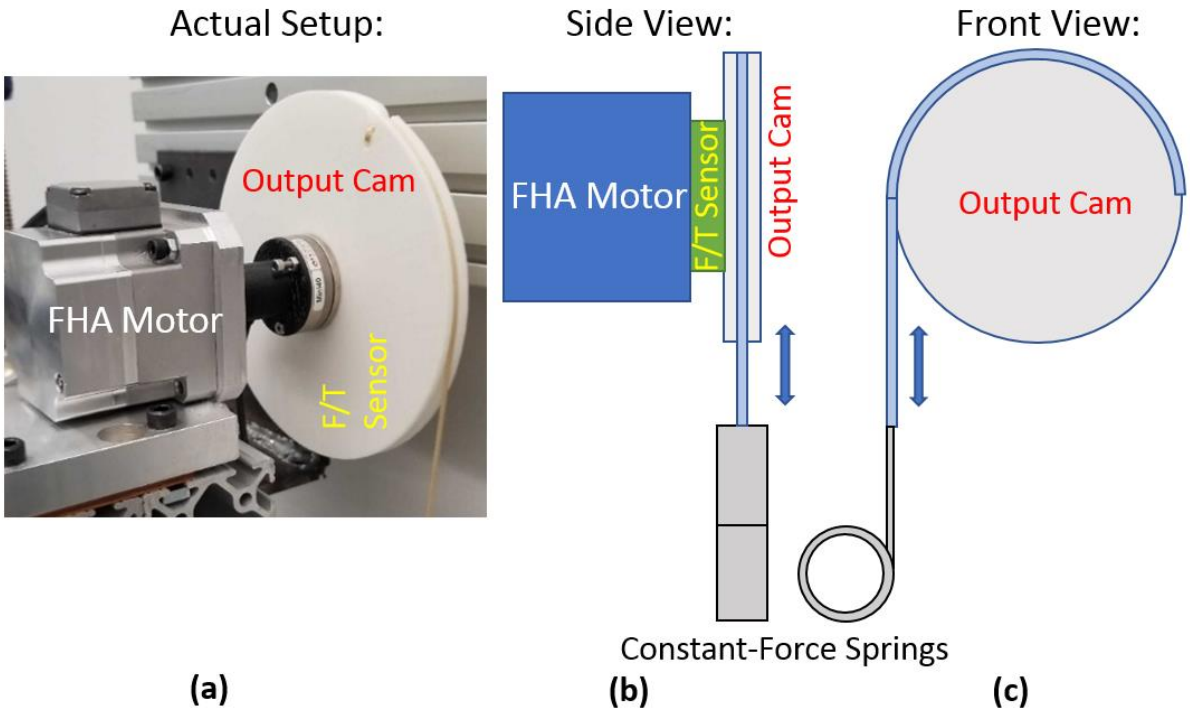

Figure 2.2. Experimental setup and hardware for force and friction testing of constant-force springs. (a) actual hardware used in the experiment, (b) a theoretical side view of the experiment, (c) a theoretical front view of the experiment.

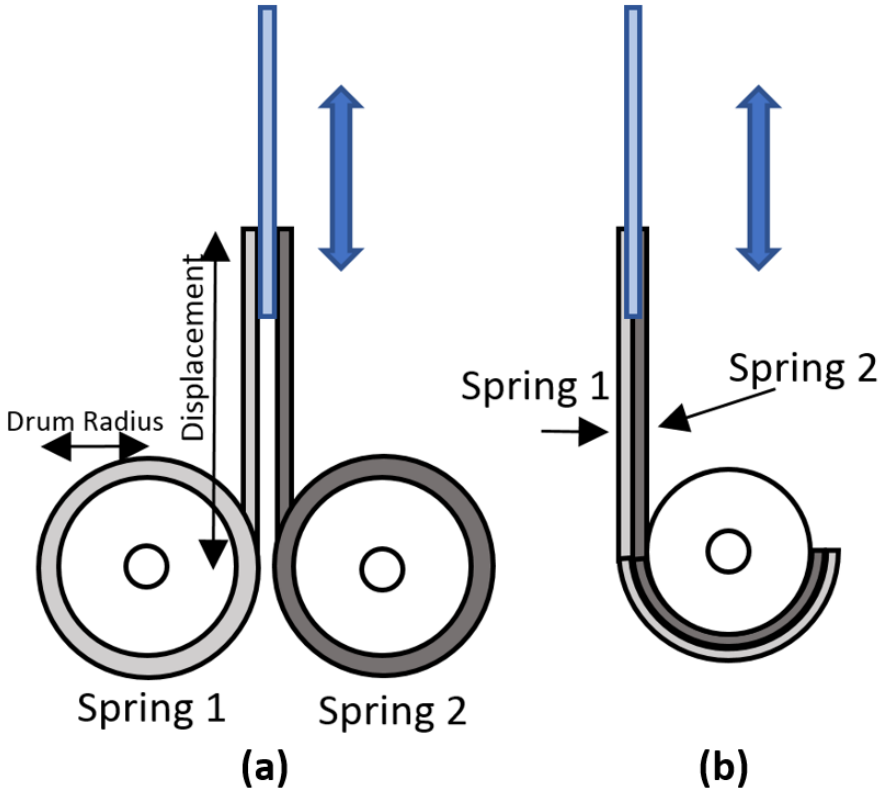

Figure 2.3. Two multiple-spring mounting configurations. (a) two springs mounted back-to-back on separate drums.(b) two springs double-wrapped on the same drum.

can reduce the total space required for the mechanism. However, these configurations may also produce unwanted force fluctuation and friction. Thus, three configurations were considered for testing: 1) a single spring (Figure 2.2, (c)), 2) two springs attached back-to-back (Figure 2.3, (a)), and 3) two springs wound together in parallel (double-wrapped, Figure 2.3, (b)). For ease of comparison, the configurations with multiple springs are normalized by dividing measured spring force by the number of springs present in each test.

The way in which the constant-force springs are mounted can have a large impact on the overall friction and can cause inaccuracies in the experimental results. Following the recommendation of the manufacturer (Vulcan Spring), the diameter of the mounting spool was sized approximately 115-120% of the inside diameter of the unstretched coiled spring. This creates enough friction to prevent the coiled spring from slipping on the mounting spool, and eliminates most of the ‘clicking’ caused by the end of the spring inside the coil passing over the point of contact on the spool. The mounting spool also utilizes shielded ball bearings to minimize friction. A final mounting consideration is the minimum displacement

of the springs for the design. The results of (Ohtsuki et al., 2001) showed that values of x/R (ratio of displacement to spring radius) of around 5 yield force results that are approximately 90% of the overall maximum force value. At lower ratios, the force output is very non-linear and increases rapidly with displacement. As a result, a minimum ratio of displacmenet to spring radius of 5 has been chosen for all tests.

2.3 Experimental Setup

The goal of the experiments is to determine the ability of constant-force springs to provide a constant torque over the required range of rotation, and to evaluate the magnitude and repeatability of hysteresis caused by friction. The experimental setup consists of a simple cam and pulley design for converting force from the constant-force springs to torque. Although this cam profile could be changed to modify the torque profile, a constant-diameter cam of 15 cm was chosen to isolate the force profiles of the springs. A diagram of the experimental apparatus is shown in Figure 2.2. An FHA-11C Harmonic Drive motor was used to rotate the cam and an ATI 6-axis force/torque sensor with uncertainty of ± 0.05 N-m was used to measure the torque applied by the cam and determine the force created by the spring. Springs with manufacturer's specified force values of 18.2 N were chosen for this test as springs with middling life span (25000 cycles with possibilities ranging from 3000 to 50000 cycles) and force production (18.2 N with possibilities ranging from <1 N to 35 N).In exoskeletons (and similar devices) for rehabilitation, the angular position and velocity of each joint can vary widely and move in an unpredictable manner. Thus, it is important to test the torque output over an appropriate range of motions. To achieve this, a series of combined sine waves were sent to the motor controllers with differing frequencies and amplitudes; an example trajectory is shown in Figure 2.4.. Every 100 seconds, the sine wave frequency was changed to create a different trajectory, and the pattern repeated 3 times. The frequencies of the trajectories were chosen as 0.25, 0.35, and 0.5 Hz, values that lie within the range of working frequencies expected for joint 3 of the BLUE SABINO device (Bitikofer, 2018 p. 28). A range of rotation of 180° was chosen as this is the required range of motion for joint 3. Simulink Real-Time was used to control the trajectory of the actuator and to collect data from the force/torque sensor and motor encoder. Since the rotation of the motor will change

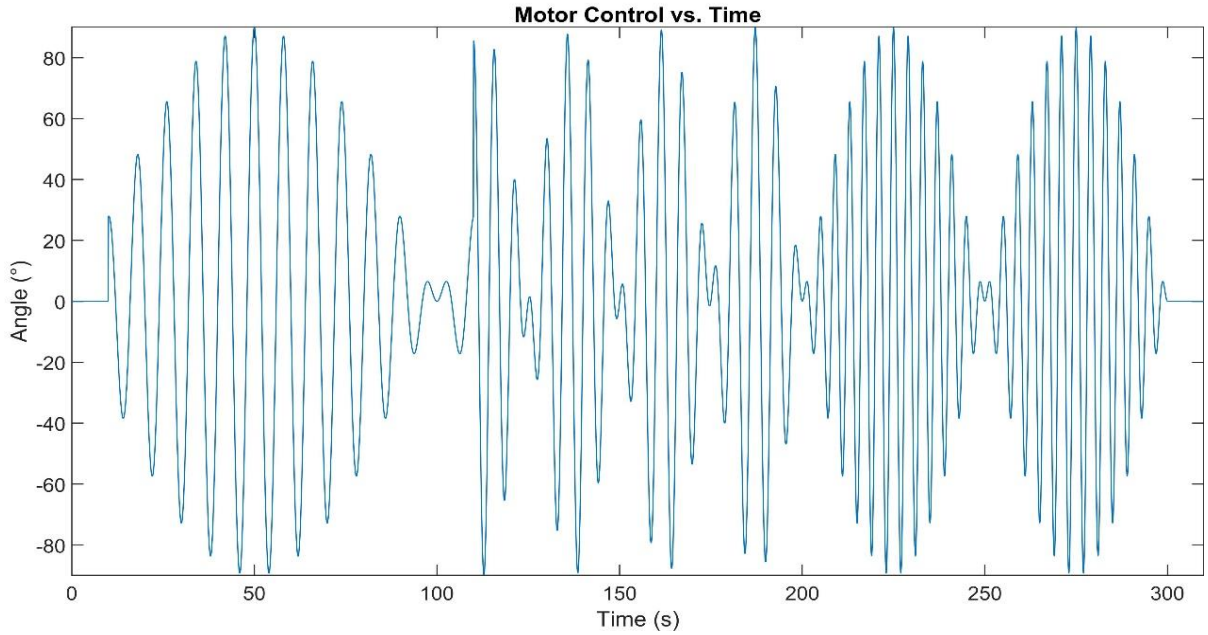

Figure 2.4. Angular trajectory for the force and hysteresis experiments using constant-force springs.

directions during normal exoskeleton motions, directional hysteresis effects will be present in the system as the force to extend and retract the springs should differ slightly due primarily to friction (Figure 2.5.). Assuming inertial affects are negligible for the prescribed motor speeds, the friction in the system can be approximated as the difference in force between the extension and retraction portions of the loop. For the purposes of this experiment, the outermost loop of the force profile will be utilized for this calculation since it represents the largest difference in force for the experiment (maximum hysteresis). The position and torque

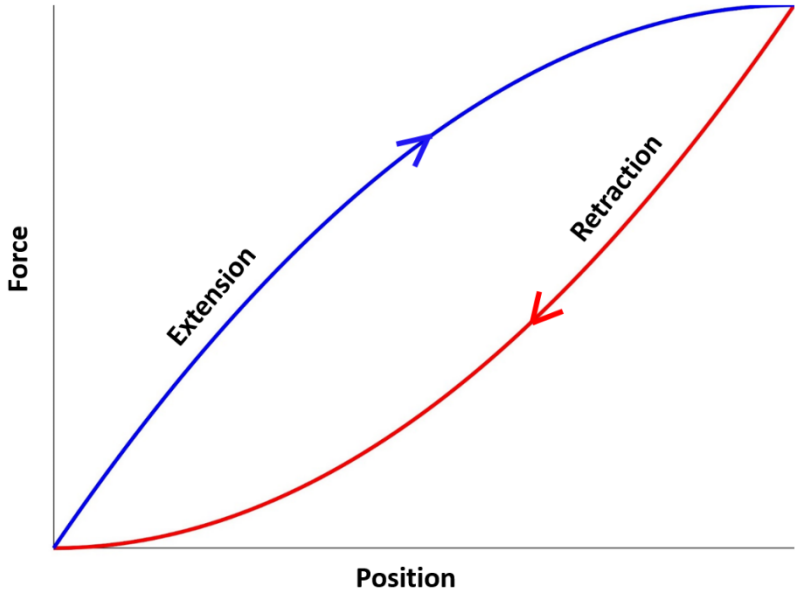

Figure 2.5. Typical hysteresis loop showing directional effects during extension and retraction.

data were smoothed with a non-causal 6th-order Butterworth low-pass filter with a cutoff frequency of 5 Hz.

2.4 Force Profiles

The magnitude and consistency of the force profiles are important properties in determining whether the use of constant-force springs in a constant-torque mechanism is viable. Tests were performed on several different spring mounting configurations and at several different rotating frequencies to determine these properties. In each experimental configuration, the torque created from the springs applied to a constant diameter cam was recorded over a range of ±90 degrees of rotation. By dividing torque by the radius of the cam, the force produced from each constant-force spring was calculated. Force output, rather than torque output, was chosen to allow for comparison to manufacturer's specifications. Figure 2.6 shows spring force vs. angular position for a typical experiment, with the axis limits of the outer plot providing a proper scaling of the near-constant force and hysteresis,

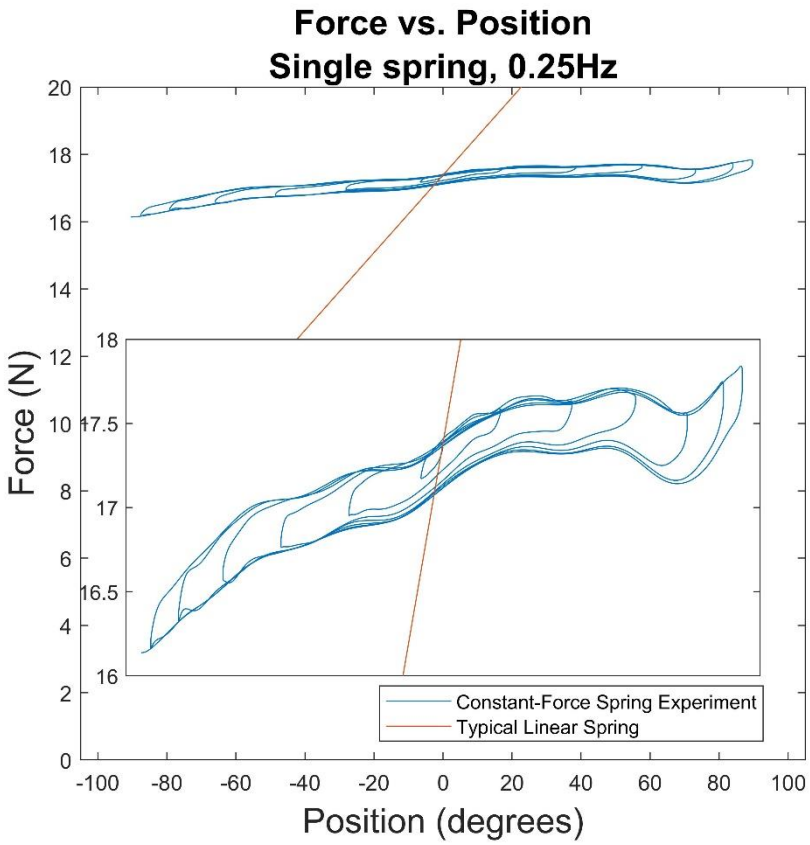

Figure 2.6. Force profile for a single spring tested at 0.25 Hz. Outer axis shows data to scale, inner axis shows a zoomed view of the same force profile. The orange line shows the theoretical force profile of a typical linear spring with a spring constant of k = 0.088 N/mm over the same displacement range.

and the inset plot providing a more detailed view of the slightly changing force profile. It also shows the theoretical force profile of a typical linear spring for comparison. The remaining plots use a similar zoomed view, but the reader should keep the scaling of the outer plot in Figure 2.6 in mind when interpreting the data.

Both spring mounting configuration (single spring, back-to-back, and double-wrapped, shown as separate columns from left to right) and frequency of oscillation (0.25, 0.35 and 0.5 Hz shown as separate rows from top to bottom), are presented in Figure 2.6. As can be seen when comparing the varying frequencies (columns of Figure 2.6), the force vs. angle profile does not vary significantly over the range of frequencies for any of the configurations.

When comparing the results from the single-spring configuration (left column), back-to-back configuration (middle column) and double-wrapped configuration (right column), the force profiles are consistent as well. For brevity, only the force profiles for the 0.5 Hz experiments are examined in depth here. From the bottom left of Figure 2.6, the single-spring force fluctuates between ~16.2 N and ~17.6 N. This equates to a fluctuation of ~8.6%. The expected value based on the manufacturer's specified force value of 18.2 N. For the back-to-back configuration (Figure 2.6, bottom middle), the results showed a fluctuation between ~16.5 N and ~17.8 N, equating to ~7.3% of the total force. The results from the double-wrapped springs experiment (Figure 2.6, bottom right) showed a force range from ~16.4 N to ~17.4 N, or approximately 7.9% of the total force. These results are summarized, with the addition of percent of expected force in Table 2.1.

Table 2.1. Spring force minimum and maximum for the three experiments. The expected force is force predicted per manufacturer's specifications

Mount Configuration	Expected Force (N)	Max Force (N)	% of expected	Min Force (N)	% of expected
Single Spring	18.2	17.6	96.5	16.2	88.8
Back-to-Back	18.2	17.8	97.3	16.6	90.7
Double-Wrapped	18.2	17.4	95.4	16.4	89.9

As can be seen in the table, each configuration ranges from around 89-91% of manufacturer's specification for minimum force generation, up to 96-97% of manufacturer's specification for maximum force generation over its range. When coupled with the initial stretch of the springs of 5 times the spool diameter, these results are consistent with the findings in (Ohtsuki et al., 2001). Similar results were found for each of the three frequencies.

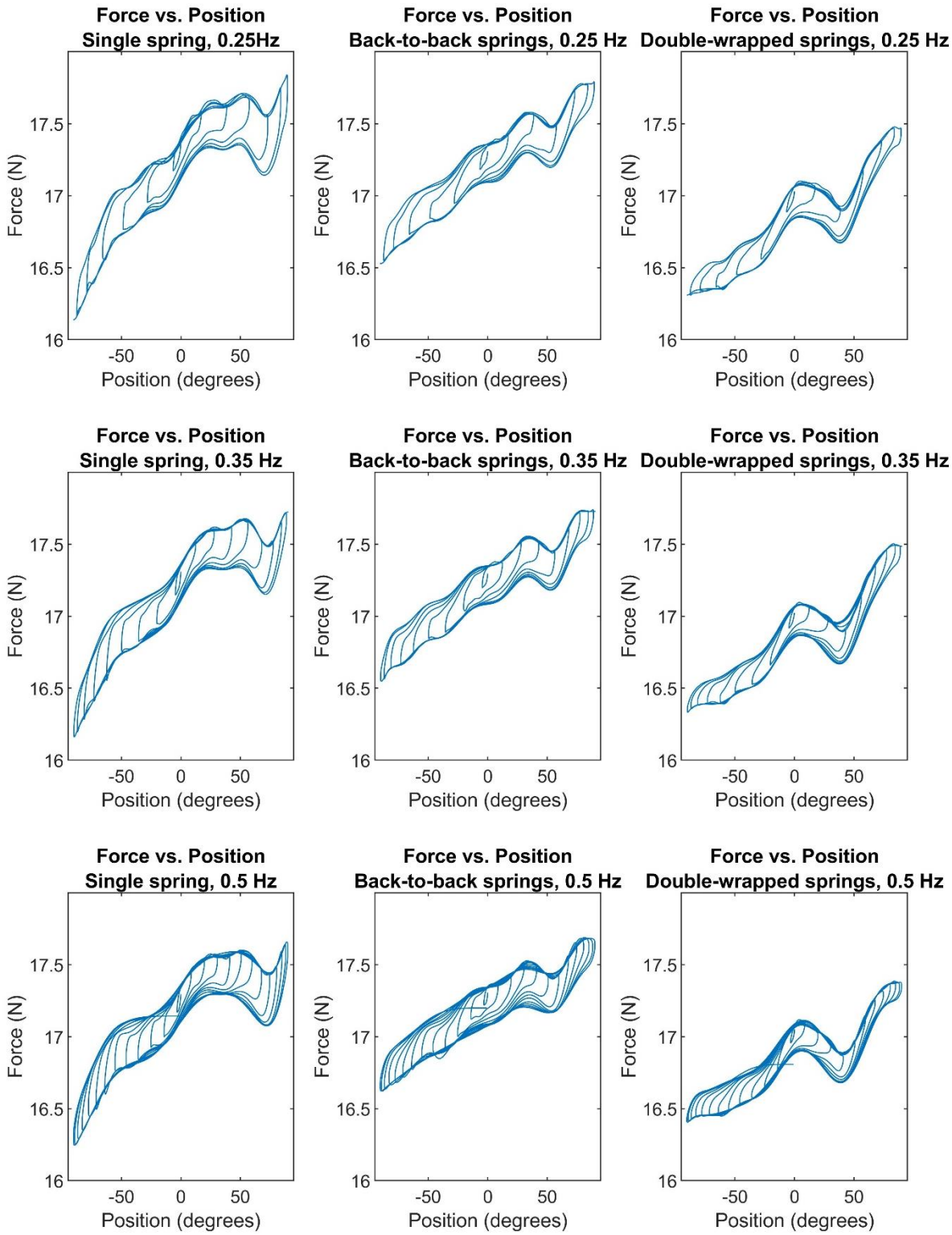

Figure 2.7. Force profiles for differing configurations and frequencies. From top to bottom, the rows correspond to 0.25, 0.35, and 0.5 Hz input frequencies. From left to right, the columns correspond to single, back-to-back, and double-wrapped configurations. The x-axis for all plots are in degrees; the y-axis for all plots is force (N) from a single spring.

The force profiles in Figure 2.6 show a general increase in force output as the angle of rotation increases (left to right). Furthermore, each force profiles show a dip in the force output curves near 60 degrees. These dips in force output are a result of the end of the spring on the mounting spool passing over the point of contact between the spool and spring. Although the spools were designed 20% oversized to limit this effect, there is still a small "bump" created as this end slips past the contact point. The dip in force output is most evident in the third experiment with double-wrapped springs (Figure 2.6, right column). This configuration creates a more significant drop in force output as a result of the essentially doubled thickness of the spring compared to the back-to-back configuration. The lack of alignment of the spring ends in the back-to-back configuration means this force output dip is distributed to two locations of the profile, resulting in a much less noticeable dip. The single spring experiment also shows this artifact clearly in the profile. These fluctuations are small in general (<1N overall) and can be neglected in many instances. If greater consistency is required, improved design of the spool mounting may be able to reduce or eliminate this artifact completely. This design would include a profile that more closely matches the inner helical shape of the spring and a way to fix the relative rotation of the spring and spool.

2.5 Friction Determination

Force vs. angle curves shown in the plots of Figure 2.6 were measured while sine waves of varying magnitude were used to control the position of the motor. These changes in magnitude caused the consistently growing loops in the datasets. Regardless of the magnitude of the sine wave, the torque returns repeatedly to an "outer" hysteresis loop at each frequency. The difference between the maximum and minimum values of this outer loop is an approximate measure of the magnitude of the static friction (assuming inertia affects are negligible). The top row of Figure 2.7 shows the outer loops for each of the three frequencies (shown as differing colors) and the different configurations (shown as differing columns). The bottom row shows the magnitude difference between the top and bottom lines (hysteresis) across the range of rotation for each of these cases. The single-spring configuration shows a maximum friction magnitude over the input range of around 0.45 N (2.7% of overall force). The back-to-back configuration showed a friction magnitude of around 0.32 N (1.9% of overall force). The third configuration with the double-wrapped springs showed a friction magnitude of 0.30 N (1.8% of overall force).

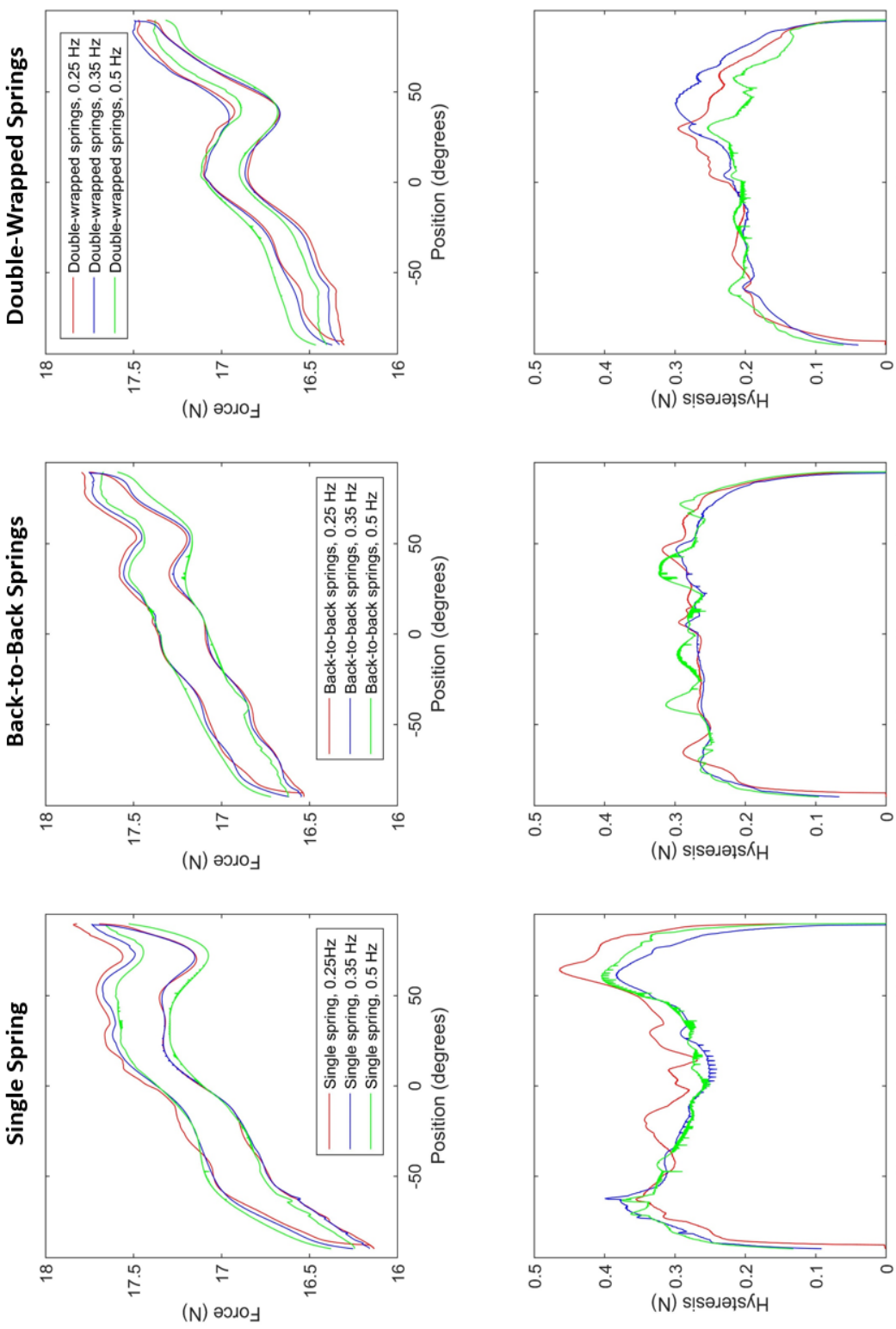

Figure 2.8. Force profiles (top) and maximum hysteresis values (bottom) over the range of rotation for the experiment (±90°). The three different configurations are shown in the three columns from left to right: (single, back-to-back (B2B) springs, and double-wrapped from left to right). Multiple input frequencies are shown for each (0.25 Hz. = red, 0.35 Hz. = blue, 0.5 Hz. = green).

2.6 Experimental Results Discussion

The goal of the experiment described in this chapter was to evaluate the potential of constant-force springs to provide constant torque to an actuated joint of an upper-extremity exoskeleton robot. In force profile and friction testing, two primary factors were considered: 1) the ability to maintain a constant torque over a typical range (±90°) of joint angles, and 2) the amount of hysteresis due to friction caused by the constant-force spring mechanism. These factors were evaluated for three different configurations: 1) single constant-force spring, 2) back-to-back springs, and 3) two springs double-wound around the same spool. Forces from the springs were converted to torques using a constant diameter cam mechanism. Furthermore, each configuration was tested at various input angle frequencies and magnitudes consistent with typical movements of the human arm.

In general, the force output profiles in the experiments, as seen in Figure 2.6, were similar for all three spring configurations. Specifically, each configuration exhibited reasonably constant force over the specified input range (±90º), with an acceptable amount of hysteresis. There were, however, small differences (±0.2 N) in the force production magnitudes for the three configurations. These differences are believed to be a result of slight twisting of the springs as they extend, which affects the force profile differently for each configuration. Further testing can verify this hypothesis, but these differences are small enough that the three configurations remain interchangeable for this application. Furthermore, the results were generally independent of input frequency over the small range appropriate for use in an exoskeleton. The largest fluctuation (~8.6%) in force vs. angle over the prescribed input range was observed from the single-spring configuration. The smallest fluctuation (~7.3%) was observed from the back-to-back configuration. Increasing the initial ratio of displacement to spring radius should only serve to make these values more consistent.

The friction magnitude values for all three configurations, shown in the bottom of Figure 2.7, are below 0.45 N for the prescribed input range. This value is acceptably low and consistent enough (below 2.7% of force for all tests) that it should have minimal impact on the overall control of the system when applied at a larger scale.

The experimental results indicate that constant-force springs are a viable candidate for the creation of a constant-torque mechanism for an exoskeleton device. The choice of mounting method, however, must be application-based. The back-to-back springs represent a simpler implementation for low force fluctuation but produce higher overall friction values than the double-wrapped springs. These factors must be considered when determining the proper configuration for a given application. With viability of constant-force springs in a constant-torque mechanism confirmed, the focus of this thesis will now shift to the design of a constant-torque mechanism using constant-force springs and its implementation into the BLUE SABINO exoskeleton.

Chapter 3: Design Implementation

The previous chapter described experiments to determine the force and friction characteristics of constant-force springs in multiple configurations, particularly as they pertain to gravity balancing of an exoskeleton joint. The results of the experiment confirm the viability of using constant-force springs in this application. This chapter presents the design and implementation of a constant-torque mechanism using constant-force springs to gravity balance joint 3 of the BLUE SABINO exoskeleton. Results from the previous chapter will be used to inform important design decisions regarding constant-force springs.

3.1 Design Implementation Constraints

Several factors govern the design of the constant-torque mechanism, including those related to constant-force springs (the results of Chapter 2) and those related to the existing design of the BLUE SABINO exoskeleton, and more specifically PRISM. Mechanisms that utilize constant-force springs require a large working range for the springs to have a sufficient minimum displacement. In addition, constant-force springs generate smaller forces than the typical linear spring, so multiple springs must be used to produce the same force. Both of these factors increase space needed for the mechanism, which must be considered when integrating the constant-force spring mechanism into the existing BLUE SABINO design.

The first major consideration in the spring design for joint 3 is the torque that must be supplied to the joint to properly balance it. From previous results from Chapter 1, a constant torque of 35 N-m at the joint will shift the center of the torque range in the motor close to zero.

The physical size of the constant-torque mechanism is another important design consideration. PRISM, the mechanism shown in Figure 3.1. has dimensions of 275 mm high x 250 mm wide x 250 mm deep. Because joint 3 comes after PRISM, the constant-torque mechanism must either be translated with the rest of the exoskeleton after joint 2, or routed

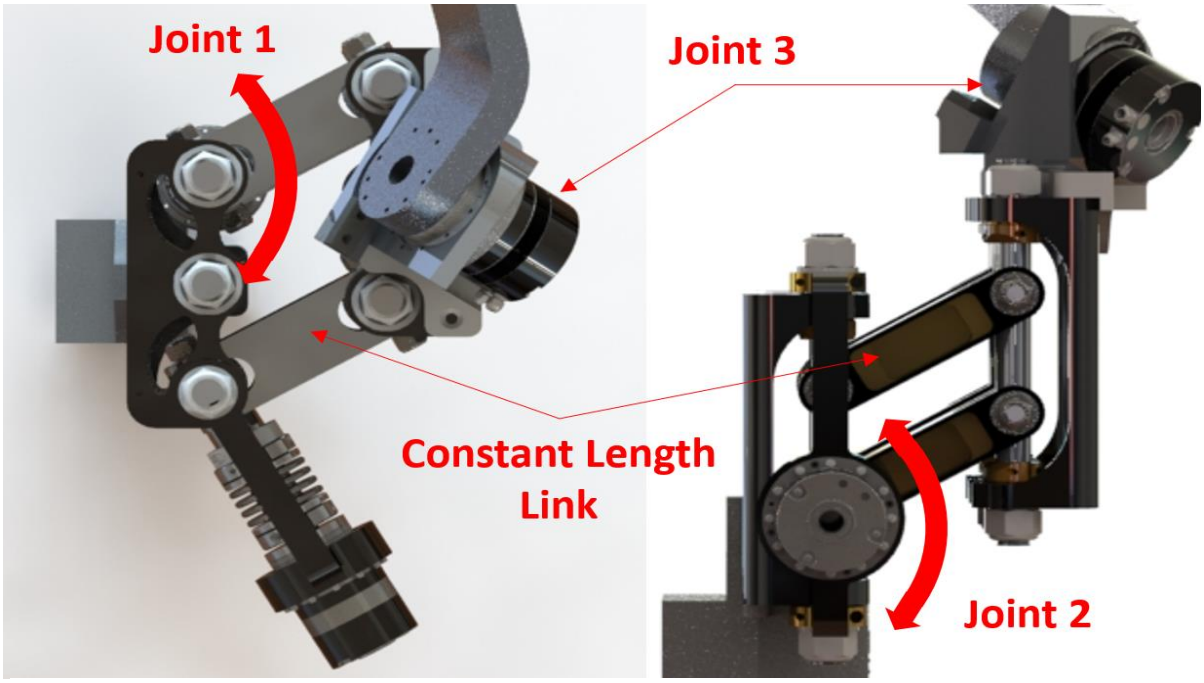

Figure 3.1. Model of PRISM on BLUE SABINO. Left: Positive rotation of joint 1. Right: Positive rotation of joint 2.

through it from the base to supply the constant 35 N-m torque to the desired location at joint 3. The nature of the design of PRISM, in which the output translates on a fixed hemispherical surface, means the lengths between components along those fixed paths never changes. This fact creates the possibility for routing a cable or other force-transferring mechanism through the device that will change minimally in length as the joints move (like the design utilized for joint 2). In this application, however, any small length change is less significant with regard to force output, as constant-force springs, not linear springs, are being used. The use of a force-carrying cable routed through PRISM allows the relocation of the bulk of the constant-torque mechanism to the base 'fixed' side of PRISM, allowing a larger mounting space as the entire base of the exoskeleton is available for use. In addition, locating the mechanism at the base of the exoskeleton means that the gravity balancing of joint 2 will not have to account for the weight of the mechanism.

Locating the constant-force mechanism at the base does not eliminate all height and width constraints, as PRISM must be positioned such that the output at joint 3 is at the proper height. Further, the nature of PRISM as a remote mechanism means its output can be anywhere and still accomplish its translation, but it must remain outside the range of motion

of the patient and robot so that collisions between the mechanism and the patient/exoskeleton cannot occur. A maximum overall height of the top of PRISM was previously chosen to be 73 cm, meaning implementation of any constant-torque mechanism cannot move PRISM above this point. Since the mechanism will have mounting considerations for both the springs and cable, 20 cm of this space must be reserved for those purposes, meaning the overall maximum displacement of the springs should be 53 cm. This means the entire range of the spring (from a minimum ratio of displacement to spring radius of 5 to the maximum extension for half of a rotation of the cam) must be contained in this space. In addition, the space between the boxes must not be restricted severely since the current design allows for a patient to enter the exoskeleton in a wheelchair. For the purposes of this design, a maximum extrusion of 7 cm on the inside of PRISM for each arm can be utilized for the new mechanism given the minimum width of 55 cm between components to fit the smallest of patients. The maximum height and minimum width dimensions discussed are shown in Figure 3.2..

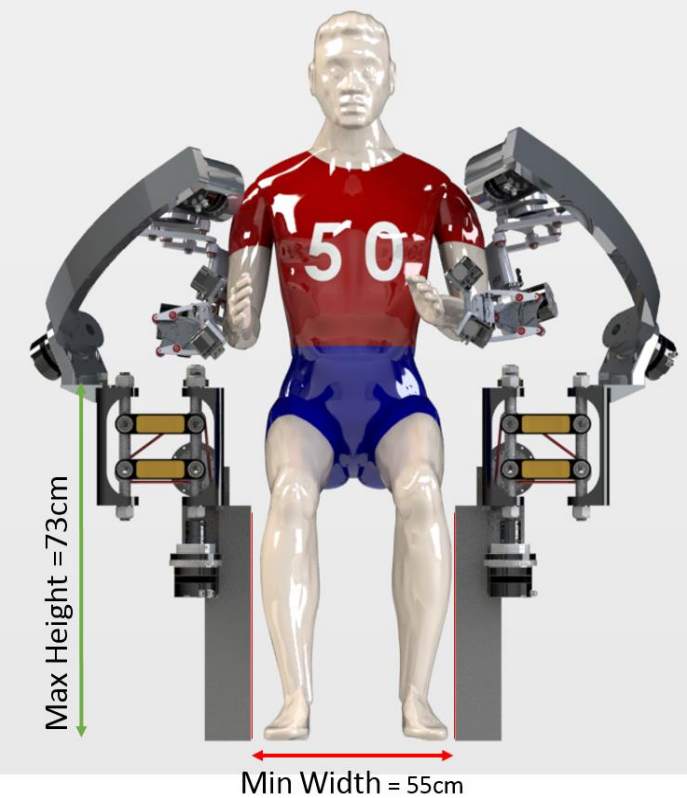

Figure 3.2. BLUE SABINO model showing minimum base width and maximum mount height constraints for the design.

The constraints described in this section will be used to govern the choices made in the design and implementation of a constant-torque mechanism to gravity balance joint 3 into the BLUE SABINO model. The remainder of this chapter will cover this design process, and the decisions made to create the mechanism.

3.2 Design Implementation: Joint 3

This section describes the physical design of the constant-force spring mechanism and its integration into the existing design of PRISM and the BLUE SABINO exoskeleton. The previous design of PRISM and the BLUE SABINO exoskeleton along with the location of joint 3 is shown in Figure 3.3. for reference.

3.2.1 Spring and Cam Selection

The torque created at the motor is a result of the product of the moment arm (radius of the cam) and the spring force. Space limitations at the actuator of joint 3 allow for a

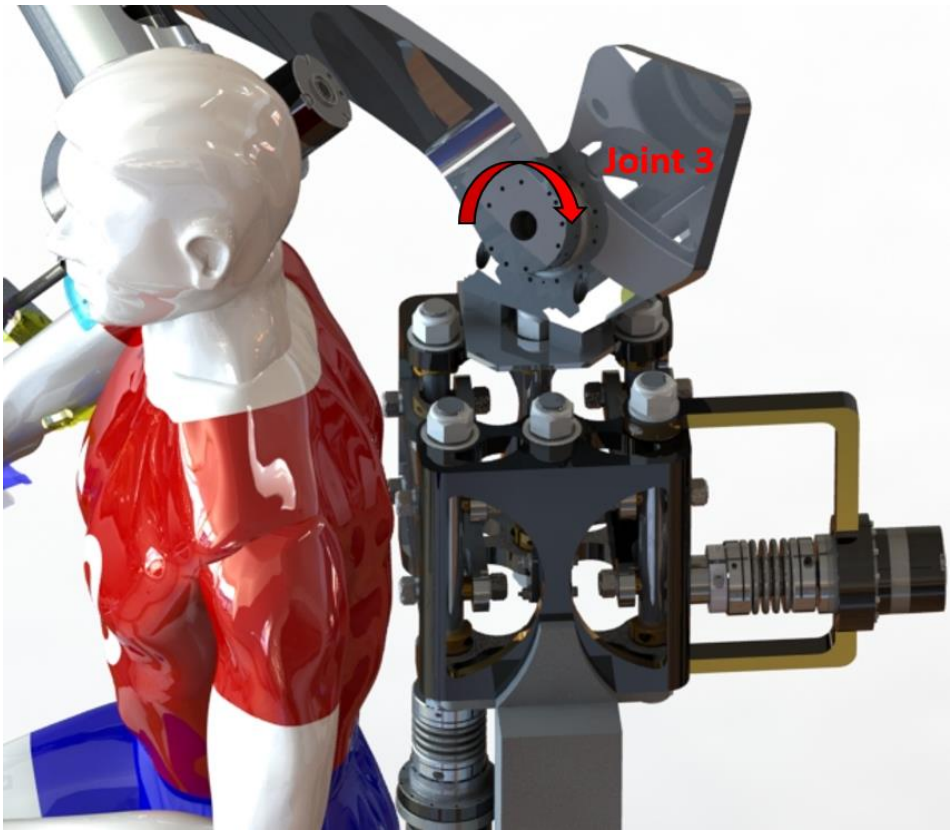

Figure 3.3. Location of joint 3 on the BLUE SABINO exoskeleton. Joint 3 combines with joints 4 and 5 to compose the 3-DOF spherical joint at the shoulder.

maximum cam radius of 10 cm. The maximum displacement of the springs was set to 53 cm, and the minimum ratio of displacement to spring radius of 5 was selected.

With these constraints, there were several choices for type and number of springs to achieve a torque output of 35 N-m. Table 3.1 shows the data utilized to select the size and number of constant-force springs for the mechanism. The range between the maximum displacement of the springs (x_{max}) and the minimum displacement (x_{min}) is used to determine the maximum radius (R) of the cam using Equation 3.1 since the displacement range is equal to the wrap length of the cam (see Figure 3.4).

$$R = (x_{max} - x_{min})/\pi \tag{3.1}$$

The minimum displacement, x_{min}, is a controllable variable chosen so that the ratio of displacement to spring radius (x/R) is a minimum of 5 to ensure sufficiently constant force generation according to (Ohtsuki et al., 2001). Use of this minimum value, however, resulted in cam radius values that were larger than 10 cm, since the range between x_{max} and x_{min} was

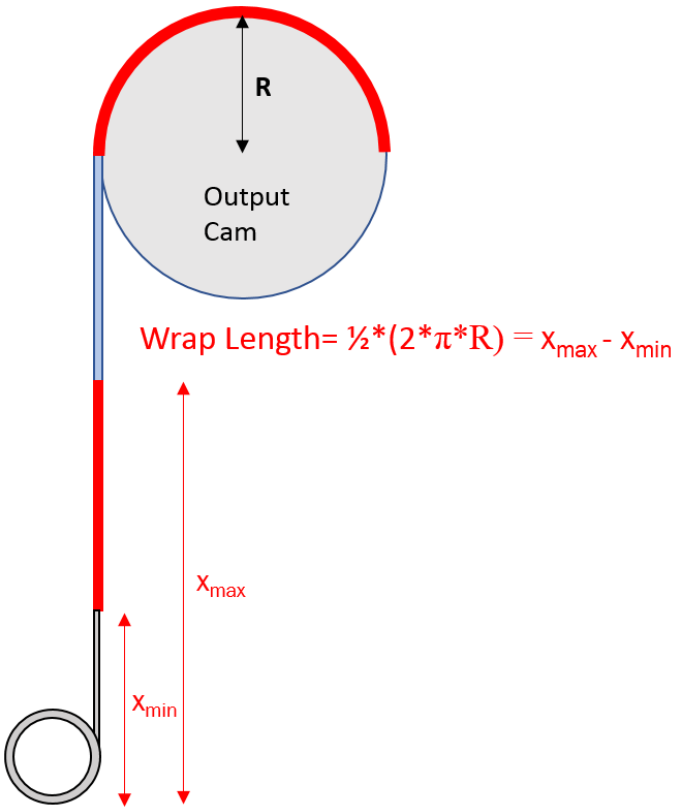

Figure 3.4. Relationship between the radius of the cam (R) and the wrap length (x_{max} - x_{min}) for the application of joint 3 gravity balancing.

so large. Consequently, the minimum value (x_{min}) was increased by a constant until the cam radius was a more reasonable size. This constant, (C), chosen as 8 cm, scales down the size of the cam radius while increasing the total number of springs needed to provide the proper torque. It is important to limit the overall spring force as much as possible, however, because larger forces from the springs (required because of a smaller mounting cam size) mean the cable and pulley assembly will see increased forces which may increase friction. Overall spring force is defined by Equation 3.2.

$$F_t = NF \tag{3.2}$$

where N is the number of springs needed to supply the constant torque (T) and F is the force produced by a single spring. A final consideration is the choice of the number of springs to use in the design. Using an even number of springs allows any component designed to transmit the force of these springs to be balanced, with an equal number of springs on opposing sides of the component.

Considering all of these factors, the 23.2 N springs were chosen (highlighted in Table 3.1). The design will use 18 of these springs wrapped on 6 individual drums (3 on each drum). The results from Section 2.4 suggest the mounting configuration has little impact on

Table 3.1. Spring and cam selection information. The overall # of springs, cam diameter, and overall spring force are considered to determine the optimum spring selection.

Force F (N)	Spring Radius R_s (cm)	Min. Initial Disp. x_{min} (cm)	Max Disp. x_{max} (cm)	Desired Torque T (N-m)	Max Cam Radius R (cm)	# of Springs N	Overall Force F_t (N)
18.2	2.8	22.0	53.0	35.0	9.9	20	364.9
15.6	2.8	22.0	53.0	35.0	9.9	23	358.2
17.2	3.3	24.7	53.0	35.0	9.0	23	395.1
19.4	2.9	22.5	53.0	35.0	9.7	19	369.5
23.2	**3.7**	**26.3**	**53.0**	**35.0**	**8.5**	**18**	**417.3**
25.9	3.6	25.9	53.0	35.0	8.6	16	415.1
32.2	4.9	32.6	53.0	35.0	6.5	17	547.7
38.9	4.7	31.5	53.0	35.0	6.8	14	544.5

the overall force profile and friction characteristics of the springs, therefore, three rows of two spools mounted back-to-back will be used.

A cam design is also needed to transmit the forces from the springs to the motor. A circular profile, like the one used in the force and friction testing, keeps the moment arm constant so that changes in the output torque can only be caused by changes in the spring force. Because the spring forces change slightly with spring displacement, a non-constant profile could be created to provide a constant 35 N-m torque at any joint angle.

The springs tested for force and friction in the experiment in Sections 2.4 and 2.5 were lower force (18.2 N) than the springs selected for the design (23.2 N). If the displacement/spring radius of different springs is consistent, however, similar profiles can be expected. Thus, the results from testing in Sections 2.4 and 2.5 will be extended to the larger springs used here.

Initial displacement of the springs was increased with a constant (C), raising the ratio of displacement to drum radius from 5 to 7 while allowing a smaller cam radius at the motor. This initial displacement has an expected force output of 95% of the manufacturer's specification. The maximum displacement to drum radius value (x/R = 14) has an expected force output of nearly 99% of the manufacturer's specification. The 18 springs in total would generate 417.3 N of force according to the manufacturer's specifications (18 springs at 23.2 N each). The actual expected force generation at minimum displacement (95% of the manufacturer's specification) and maximum displacement (99% of the manufacturer's specification) are 396.4 N and 413.2 N respectively. The cam radius to achieve a constant 35 N-m torque at the motor would then need to change from 8.83 cm at minimum spring displacement, to 8.47cm at maximum spring displacement. The increase in initial displacement means that the force fluctuation of this configuration is small (20 N, ~ 5%). For that reason, the implementation of a changing cam radius in this design is not included. Using a circular cam will allow for clearer results when testing the initial design, and if a cam is still desired, it can be implemented at that time. The resulting overall torque from the springs with a circular cam is expected to be 35.0±0.7 N-m over the entire displacement range of the springs for a cam with radius 8.65 cm.

3.2.2 Base Mount

The 18 constant-force springs used in the design can be wrapped onto six individual drums with three springs wrapped on each drum using the configuration shown in Figure 3.5.. As specified in the methods section, spool OD's are over-sized to 115-120% of the spring diameter. A series of threaded shafts are used to connect each set of three drums and attach them to the mounting structure for the springs.

This mounting structure is designed to contain and properly space the spring drums and must fit within the size constraints discussed in Section 3.1. The springs are oriented to maximize the available space below the device and utilize the height of PRISM for part for the displacement range. The structure also includes a guide system for the spring/cable attachment (presented in section 3.2.3) to keep the motion of the end of the springs vertical and ensure that all springs extend simultaneously. An image of this base mechanism, along with an internal view of the springs in the mechanism is shown in Figure 3.5..

Figure 3.5. Housing structure for constant-force spring coils including extension guides. Left shows the springs connected to the guide system. Right shows the complete assembly.

3.2.3 Spring/Cable Attachment

A component was created to connect the 18 springs (on 6 individual coils) to the cable to transmit the forces. The mount is designed to withstand the maximum forces expected from the springs (420N) while ensuring proper alignment of the springs. The component implemented into the base design, showing the use of the guide rails is shown in Figure 3.6.

Overall, the mechanism utilizes 18 constant-force springs with manufacturers' specified force values of 23.2 N per spring. The cam, cable, and spring configuration are chosen to maximize the utility of the available space below PRISM. The resulting forces from the springs coupled with the cam at the motor mount were designed to provide close to 35 N-m of torque to the joint at any orientation of PRISM and any angle of rotation of joint 3.

3.2.4 Cable Routing

Connecting the output of the spring mechanism to the 3rd joint of the BLUE SABINO exoskeleton requires routing a cable through PRISM. The current design of PRISM includes a spring balancing mechanism for joint 2 (Trimble, 2016), which must be altered to allow the cable routing for the joint 3 gravity-balancing mechanism. The balancing mechanism for joint 2 must also be implemented in the final design, but the integration of the two is outside the scope of this work. Figure 3.7 shows the routing of the cable from the constant-torque mechanism to joint 3 of the BLUE SABINO exoskeleton. Pulley 1 (Figure 3.7 (a)) is located to allow additional displacement height of the springs and transmit the cable from the spring

Figure 3.6. Spring/cable attachment for force transmission. Designed to transmit the force from 6 individual spools to a cable that can be routed through PRISM.

mechanism directly down the axis of rotation of joint 1 to pulley 2. Pulley 2 is mounted such that the cable maintains collinearity with joint axis 1 as it transfers from pulley 1 to pulley 2. A similar alignment occurs between pulleys 3 and 4. Pulleys 2 and 3 are mounted on an internal link that rotates with joint 1, but in specific locations that ensure that the alignment to their respective vertical pulleys does not change when joint 1 rotates. In other words, the cable between pulleys 1 and 2 does not change orientation as joint 1 is actuated, and likewise for the cable between pulleys 3 and 4.

Typical pulley/cable assemblies for gravity-balancing used in general four-bar mechanisms would locate the axis of rotation of pulley 2 on the axis of joint 1. These devices rotate in-plane, which would be similar to PRISM with the exclusion of joint 1. This typical configuration would come with the benefit of constant cable length between pulleys 2 and 3 during rotations of joint 2 since wrapping on one pulley directly unwraps the other. The nature of the dual four-bar mechanism used in the design of PRISM, however, complicates this design with the inclusion of rotation of joint 1. Mounting the axis of rotation of pulley 2

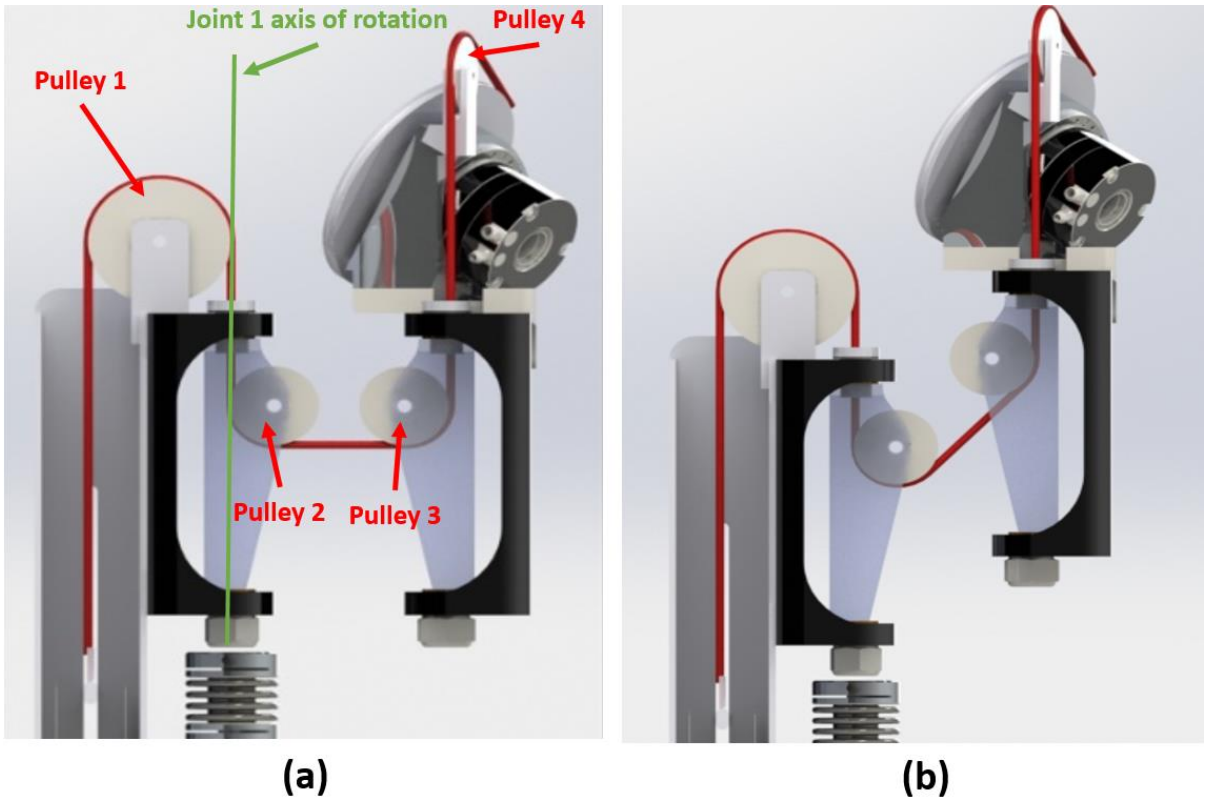

Figure 3.7. Full cable routing from the spring mechanism to the output at joint 3. (a) The routing at 0° of rotation for joint 2. (b) The routing at 30° of rotation for joint 2.

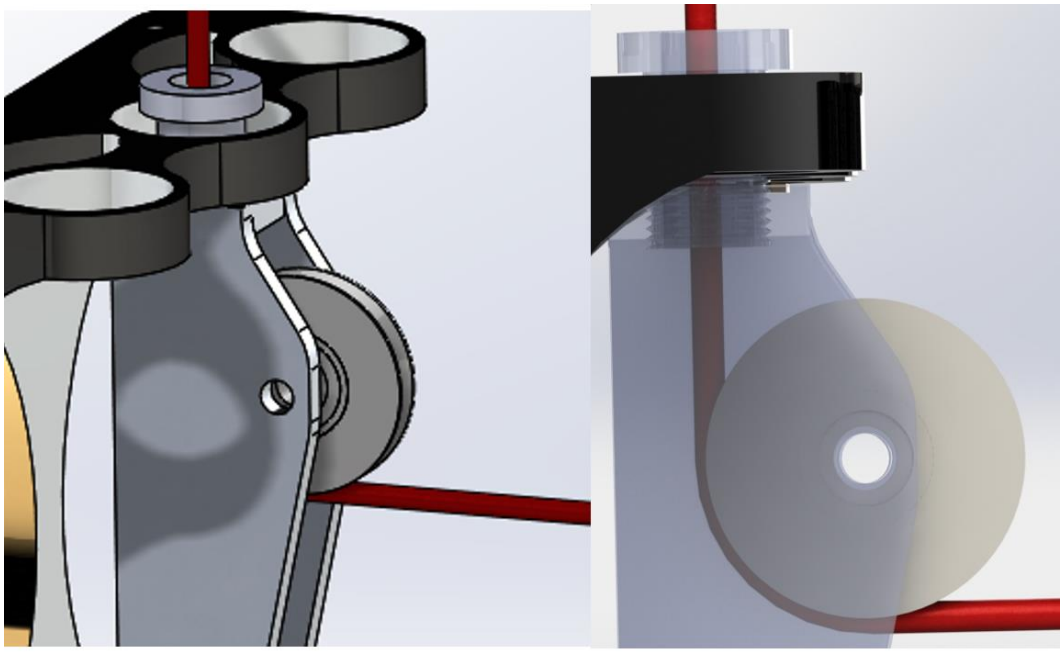

Figure 3.8. (a) New component and screw cap used to allow the routing of the cable through its center. (b) Transparent view of this component to visualize cable routing.

on the axis of joint 1 in this case makes routing of the cable more difficult between pulleys 1 and 2 since the cable no longer remains collinear with the joint 1 axis and instead moves as the joint rotates. This can be more easily visualized in the images from Figure 3.8. A slight fluctuation in cable length in an application with constant-force springs is much less impactful than in a typical spring balancing mechanism as well, because a very small length change results in a negligible change in force from the springs. For these reasons, the pulleys were mounted with their edges on the cable routing axis to simplify the overall cable routing in the design as shown in Figure 3.7 and Figure 3.8.

The mounting of the pulleys in this manner creates the need to route the cable in from the top or bottom of PRISM directly through the axis of rotation of joint 1 to take advantage of the simplified mounting. A component was created to take place of the aluminum shafts from the previous design that would allow a cable down its center axis. This component and its mounting screw are shown in Figure 3.8.

All of the components from this section were combined and integrated into the BLUE SABINO exoskeleton CAD model. A rendering of the resulting base structure combined with PRISM is shown in Figure 3.9. The mechanism should provide a torque of 35.0 ± 0.7 N-m to joint 3 of the BLUE SABINO exoskeleton at every angle of rotation of joints 1, 2, and 3.

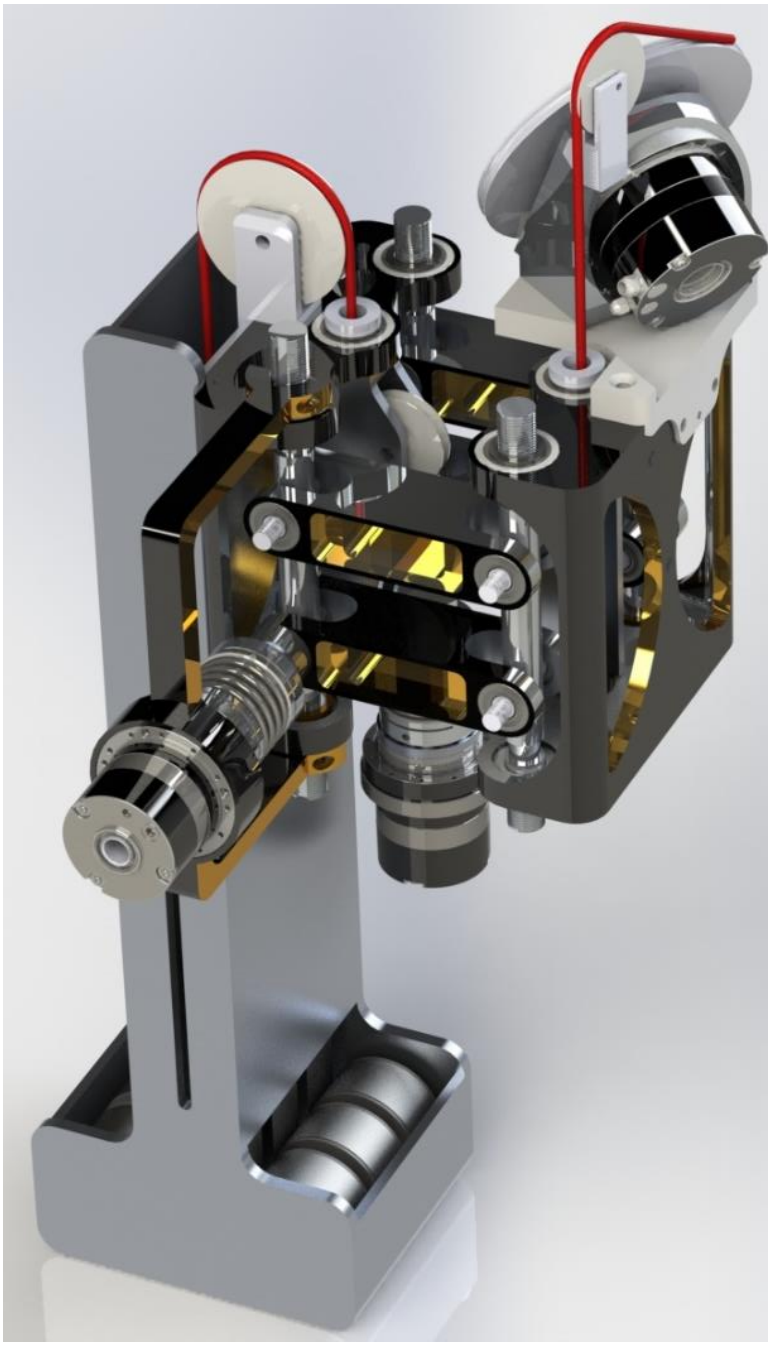

Figure 3.9. Full constant-force spring and cam assembly integrated into the existing design of PRISM (joints 1 and 2) and joint 3 of the BLUE SABINO exoskeleton.

3.3 Design Discussion

The addition of a constant-torque mechanism to gravity balance joint 3 of the BLUE SABINO exoskeleton was presented in this chapter. Previous design of a gravity compensation device for joint 2 (Trimble, 2016) had included space in PRISM for the routing of cables and placement of pulleys to accommodate this gravity balancing. Eighteen springs with manufacturers' specified force of 23.2 N each were selected based on available size, maximum cam diameter, overall force generation, and number of springs needed to provide the force for the mechanism. A base structure and spring mounting component were created to withstand the forces from the springs and transmit the forces to the cable/pulley assembly. The routing of the cable for transmission of forces was accomplished with the inclusion of 4 pulleys into the current PRISM design with consideration given to maintaining collinearity of the cable to joint 1 to minimize cable movement and design complexity during joint rotation. A small amount of cable length change is expected because of this decision, but this length change should not impact the force generation of the mechanism heavily as the force of these constant-force springs in the designed displacement range should be very consistent. The resulting design for the mechanism fits within the size constraints of the base and should apply a torque of 35.0 ± 0.7N-m to the actuator at joint 3. Simply adding or removing springs or changing the type of spring used in the mechanism can greatly change the torque production capabilities, allowing versatility to the design for many torque balancing applications. Additionally, if a more constant torque profile or a specific shape of force profile is desired at the joint, the attachment cam can be customized to modify the generated torque profile.

Chapter 4: Conclusion

The goal of the work described in this thesis was to investigate the force profile and friction characteristics of constant-force springs and develop a passive constant-torque mechanism using constant-force springs to gravity balance joint 3 of the BLUE SABINO exoskeleton. This chapter will cover some potential sources of error in the experimentation and design of the constant-torque mechanism, include possible future work to move the mechanism closer to a finished product, and provide some closing remarks with respect to the mechanism.

4.1 Potential sources of error

Additional consideration should be given to another of the characteristics of the constant-force springs not tested in this thesis. Resonance as a result of stick-and-slip friction is a possible concern for constant-force springs. When the springs undergo quick changes in displacement, it is likely that artifacts from resonance may appear in the force profiles for the springs. It is also possible that the frequency of this resonance changes as a function of the displaced length of the springs. Further experimentation is needed to determine the impact of resonance on the system, but no artifacts were easily observed from the data to suggest it may be a major problem.

4.2 Future Work

This thesis presented results from force profile and friction testing of constant-force springs, and the design and implementation of a conceptual model into the BLUE SABINO exoskeleton to provide gravity balancing to joint 3. Additional efforts will be needed, however, to ensure the design is ready to be built and utilized in the exoskeleton. First, more testing on the springs should be completed that includes resonance testing as discussed above. This additional testing should cover a larger range of springs to ensure that the force profiles and friction characteristics are consistent when changing the size of spring used in the test. In addition, this testing should verify the cause of the slight fluctuation in force magnitude between the three configurations, expected to be caused by the twisting of the springs as they extend, and any design using the springs should compensate for these

differences. Next, selection of bearings, fasteners, standard components, etc. for the design to be implemented properly into PRISM will be needed, along with some potential minor design changes to fit these components. Finally, once the force profile for the mechanism itself is more clearly understood, a cam design can be implemented to ensure the torque from the mechanism remains constant at the joint during use.

4.3 Concluding Remarks

Overall, the force and friction profiles of constant-force springs indicate they are a viable option to create relatively large constant torques when coupled with proper spring selection and cam design. These results led to the prototyping of a constant-torque mechanism for joint 3 of BLUE SABINO to supply 35.0 ± 0.7 N-m of torque to the motor at the joint. The design to this point is conceptual, with manufacturing and testing still needed to verify the mechanism. That being said, the design represents a simple solution to the problem of gravity balancing present in many exoskeleton devices, and the concepts developed here can be applied in a large range of applications.

References

American Heart Association, 2019. Heart Disease and Stroke Statistics—2019 Update: A Report From the American Heart Association 473.

Ball, S.J., Brown, I.E., Scott, S.H., 2007. MEDARM: a rehabilitation robot with 5DOF at the shoulder complex, in: 2007 IEEE/ASME International Conference on Advanced Intelligent Mechatronics. Presented at the 2007 IEEE/ASME international conference on advanced intelligent mechatronics, pp. 1–6. https://doi.org/10.1109/AIM.2007.4412446

Bitikofer, C.K., 2018. Mapping ADL Motion Capture Data to BLUE SABINO Exoskeleton Kinematics and Dynamics. University of Idaho.

Bitikofer, C.K., Hill, P.W., Wolbrecht, E.T., Perry, J.C., 2019. Analysis of Shoulder Displacement During Activities of Daily Living and Implications on Design of Exoskeleton Robotics for Assessment, in: Masia, L., Micera, S., Akay, M., Pons, J.L. (Eds.), Converging Clinical and Engineering Research on Neurorehabilitation III, Biosystems & Biorobotics. Springer International Publishing, pp. 478–482.

Chung, D.G., Hwang, M., Won, J., Kwon, D., 2016. Gravity compensation mechanism for roll-pitch rotation of a robotic arm, in: 2016 IEEE/RSJ International Conference on Intelligent Robots and Systems (IROS). Presented at the 2016 IEEE/RSJ International Conference on Intelligent Robots and Systems (IROS), pp. 338–343. https://doi.org/10.1109/IROS.2016.7759076

Colombo, R., Pisano, F., Micera, S., Mazzone, A., Delconte, C., Carrozza, M.C., Dario, P., Minuco, G., 2005. Robotic techniques for upper limb evaluation and rehabilitation of stroke patients. IEEE Trans. Neural Syst. Rehabil. Eng. 13, 311–324. https://doi.org/10.1109/TNSRE.2005.848352

Feigin, V.L., Forouzanfar, M.H., Krishnamurthi, R., Mensah, G.A., Connor, M., Bennett, D.A., Moran, A.E., Sacco, R.L., Anderson, L., Truelsen, T., O'Donnell, M., Venketasubramanian, N., Barker-Collo, S., Lawes, C.M.M., Wang, W., Shinohara, Y., Witt, E., Ezzati, M., Naghavi, M., Murray, C., 2014. Global and regional burden

of stroke during 1990–2010: findings from the Global Burden of Disease Study 2010. The Lancet 383, 245–255. https://doi.org/10.1016/S0140-6736(13)61953-4

Guidali, M., Schmiedeskamp, M., Klamroth, V., Riener, R., 2009. Assessment and training of synergies with an arm rehabilitation robot, in: 2009 IEEE International Conference on Rehabilitation Robotics. Presented at the 2009 IEEE International Conference on Rehabilitation Robotics, pp. 772–776. https://doi.org/10.1109/ICORR.2009.5209516

Herder, J.L., 2001. Energy-free Systems; Theory, conception and design of statically balanced spring mechanisms. https://doi.org/10.13140/rg.2.1.3942.8966

ja.pdf, n.d.

Kim, B., Deshpande, A.D., 2017. An upper-body rehabilitation exoskeleton Harmony with an anatomical shoulder mechanism: Design, modeling, control, and performance evaluation. Int. J. Robot. Res. 36, 414–435. https://doi.org/10.1177/0278364917706743

Kwakkel, G., Kollen, B., Lindeman, E., 2004. Understanding the pattern of functional recovery after stroke: Facts and theories. Restor. Neurol. Neurosci. 22, 281–299.

Langhorne, P., Bernhardt, J., Kwakkel, G., 2011. Stroke rehabilitation. The Lancet 377, 1693–1702. https://doi.org/10.1016/S0140-6736(11)60325-5

Lee, D., Seo, T., 2017. Lightweight Multi-DOF Manipulator With Wire-Driven Gravity Compensation Mechanism. IEEEASME Trans. Mechatron. 22, 1308–1314. https://doi.org/10.1109/TMECH.2017.2681102

Mistry, M., Mohajerian, P., Schaal, S., 2005. An exoskeleton robot for human arm movement study, in: 2005 IEEE/RSJ International Conference on Intelligent Robots and Systems. Presented at the 2005 IEEE/RSJ International Conference on Intelligent Robots and Systems, pp. 4071–4076. https://doi.org/10.1109/IROS.2005.1545450

Norouzi-Gheidari, N., Archambault, P.S., Fung, J., 2012. Effects of robot-assisted therapy on stroke rehabilitation in upper limbs: Systematic review and meta-analysis of the literature. J. Rehabil. Res. Dev. 49, 479. https://doi.org/10.1682/JRRD.2010.10.0210

Ohtsuki, A., Ohshima, S., Itoh, D., 2001. Analysis on Characteristics of a C-Shaped Constant-Force Spring with a Guide. Mech. Syst. Mach. Elem. Manuf., C 44, 494–499.

Ortman, J., Velkoff, V., Hogan, H., 2014. An Aging Nation: The Older Population in the United States. United States Census Bureau, Economics and Statistics Administration, US Department of Commerce 28.

Park, H.-S., Ren, Y., Zhang, L.-Q., 2008. IntelliArm: An exoskeleton for diagnosis and treatment of patients with neurological impairments, in: 2008 2nd IEEE RAS EMBS International Conference on Biomedical Robotics and Biomechatronics. Presented at the 2008 2nd IEEE RAS EMBS International Conference on Biomedical Robotics and Biomechatronics, pp. 109–114. https://doi.org/10.1109/BIOROB.2008.4762876

Perry, J.C., Bitikofer, C.K., Hill, P.W., Wolbrecht, E.T., 2018. Development of a 2-DOF Dual-Four-Bar Exoskeleton Shoulder Mechanism to Support Elevation, Depression, Protraction, and Retraction, in: Wearable Robotics: Systems and Applications. Ed. Jacob Rosen, Elsevier.

Perry, J.C., Maura, R., Bitikofer, C.K., Wolbrecht, E.T., 2019. BLUE SABINO: Development of a Bilateral Exoskeleton Instrument for Comprehensive Upper-Extremity Neuromuscular Assessment, in: Masia, L., Micera, S., Akay, M., Pons, J.L. (Eds.), Converging Clinical and Engineering Research on Neurorehabilitation III, Biosystems & Biorobotics. Springer International Publishing, pp. 493–497.

Prange, G.B., Jannink, M.J.A., Groothuis-Oudshoorn, C.G.M., Hermens, H.J., IJzerman, M.J., 2006. Systematic review of the effect of robot-aided therapy on recovery of the hemiparetic arm after stroke. J. Rehabil. Res. Dev. 43, 171. https://doi.org/10.1682/JRRD.2005.04.0076

Rahman, M.H., Ouimet, T.K., Saad, M., Kenné, J.P., Archambault, P.S., 2010. Development and control of a wearable robot for rehabilitation of elbow and shoulder joint movements, in: IECON 2010 - 36th Annual Conference on IEEE Industrial Electronics Society. Presented at the IECON 2010 - 36th Annual Conference on IEEE Industrial Electronics Society, pp. 1506–1511. https://doi.org/10.1109/IECON.2010.5675459

Rahman, T., Ramanathan, R., Seliktar, R., Harwin, W., 1995. A Simple Technique to Passively Gravity-Balance Articulated Mechanisms. J. Mech. Des. 117, 655. https://doi.org/10.1115/1.2826738

Rahman, T., Sample, W., Jayakumar, S., King, M.M., Wee, J.Y., Seliktar, R., Alexander, M., Scavina, M., Clark, A., 2006. Passive exoskeletons for assisting limb movement. J. Rehabil. Res. Dev. 43, 583. https://doi.org/10.1682/JRRD.2005.04.0070

Rahman, T., Sample, W., Seliktar, R., 2004. 16 Design and Testing of WREX, in: Bien, Z.Z., Stefanov, D. (Eds.), Advances in Rehabilitation Robotics: Human-Friendly Technologies on Movement Assistance and Restoration for People with Disabilities, Lecture Notes in Control and Information Science. Springer Berlin Heidelberg, Berlin, Heidelberg, pp. 243–250. https://doi.org/10.1007/10946978_16

Shen, Y., Ma, J., Dobkin, B., Rosen, J., 2018. Asymmetric Dual Arm Approach For Post Stroke Recovery Of Motor Functions Utilizing The EXO-UL8 Exoskeleton System: A Pilot Study, in: 2018 40th Annual International Conference of the IEEE Engineering in Medicine and Biology Society (EMBC). Presented at the 2018 40th Annual International Conference of the IEEE Engineering in Medicine and Biology Society (EMBC), pp. 1701–1707. https://doi.org/10.1109/EMBC.2018.8512665

Simkins, M., Kim, H., Abrams, G., Byl, N., Rosen, J., 2013. Robotic unilateral and bilateral upper-limb movement training for stroke survivors afflicted by chronic hemiparesis, in: 2013 IEEE 13th International Conference on Rehabilitation Robotics (ICORR). Presented at the 2013 IEEE 13th International Conference on Rehabilitation Robotics (ICORR), pp. 1–6. https://doi.org/10.1109/ICORR.2013.6650506

Tran, V.D., Dario, P., Mazzoleni, S., 2018. Kinematic measures for upper limb robot-assisted therapy following stroke and correlations with clinical outcome measures: A review, in: Medical Engineering & Physics. Elsevier Ltd., pp. 13–31. https://doi.org/10.1016/j.medengphy.2017.12.005

Trimble, S., 2016. PANDORA: Design of a 2 DOF Scapulohumeral Device. University of Idaho, Moscow, Idaho.

Yang, Q., Botto, L.D., Erickson, J.D., Berry, R.J., Sambell, C., Johansen, H., Friedman, J.M., 2006. Improvement in Stroke Mortality in Canada and the United States, 1990 to 2002. American Heart Association.